ARTICLE

Apical polarity proteins recruit the RhoGEF Cysts to promote junctional myosin assembly

Jordan T. Silver[1]* , Frederik Wirtz-Peitz[2]* , Sérgio Simões[1]*, Milena Pellikka[1]*, Dong Yan[2] , Richard Binari[2], Takashi Nishimura[4], Yan Li[1], Tony J.C. Harris[1], Norbert Perrimon[2,3], and Ulrich Tepass[1]

The spatio-temporal regulation of small Rho GTPases is crucial for the dynamic stability of epithelial tissues. However, how RhoGTPase activity is controlled during development remains largely unknown. To explore the regulation of Rho GTPases in vivo, we analyzed the Rho GTPase guanine nucleotide exchange factor (RhoGEF) Cysts, the *Drosophila* orthologue of mammalian p114RhoGEF, GEF-H1, p190RhoGEF, and AKAP-13. Loss of Cysts causes a phenotype that closely resembles the mutant phenotype of the apical polarity regulator Crumbs. This phenotype can be suppressed by the loss of basolateral polarity proteins, suggesting that Cysts is an integral component of the apical polarity protein network. We demonstrate that Cysts is recruited to the apico-lateral membrane through interactions with the Crumbs complex and Bazooka/Par3. Cysts activates Rho1 at adherens junctions and stabilizes junctional myosin. Junctional myosin depletion is similar in Cysts- and Crumbs-compromised embryos. Together, our findings indicate that Cysts is a downstream effector of the Crumbs complex and links apical polarity proteins to Rho1 and myosin activation at adherens junctions, supporting junctional integrity and epithelial polarity.

Introduction

Epithelial cells show pronounced apical-basal polarity and form an apical junctional complex that encircles individual cells and tightly links neighboring cells into a sheet-like tissue. Factors that regulate apical-basal polarity, and in particular apical polarity proteins such as Crumbs (Crb) or atypical protein kinase C (aPKC), play a pivotal role in the formation of the junctional belt. Consequently, compromising apical polarity protein function causes a loss of epithelial integrity similar to the loss of core junctional proteins such as E-cadherin (Tepass, 2012). How the function of apical polarity proteins supports a circumferential junctional belt is not well understood. One key mechanism that promotes junctional stability is the activity of cytoplasmic myosin II that is activated at apical junctions through the Rho-Rock pathway (Mack and Georgiou, 2014; Lecuit and Yap, 2015). Here, we ask how apical polarity proteins help to confine the activity of Rho1 to the apical junctional region to promote the formation of a junctional belt.

Rho GTPases are molecular switches that cycle between active (GTP-bound) and inactive (GDP-bound) states. Rho GTPases are used over and over again to regulate diverse molecular processes within cells including cytoskeletal dynamics, cell

polarity, cell adhesion, and vesicle trafficking (Jaffe and Hall, 2005; Hall, 2012; Ridley, 2012; Ratheesh et al., 2013; Mack and Georgiou, 2014). For example, epithelial polarity in the *Drosophila melanogaster* embryo requires three members of the Rho protein family: Cdc42 promotes apical polarity by activation of the apical Par protein complex (Par6/aPKC; Hutterer et al., 2004; Harris and Tepass, 2008, 2010), Rac1 acts together with phosphoinositide 3-kinase as a basolateral polarity protein (Chartier et al., 2011), and Rho1 (RhoA in mammals) supports integrity of apical adherens junctions (AJs) by activating myosin II through the Rho kinase pathway (Magie et al., 1999; Fox et al., 2005; Matsuoka and Yashiro, 2014; Lecuit and Yap, 2015).

Rho GTPase-specific guanine nucleotide exchange factors (RhoGEFs) and Rho GTPase-activating proteins (RhoGAPs) promote activation and deactivation, respectively, of Rho GTPases (McCormack et al., 2013; Cook et al., 2014). The *Drosophila* genome encodes 26 RhoGEFs and 22 RhoGAPs that presumably regulate Rho GTPases and a wide variety of downstream effectors, many of which modulate cytoskeletal remodeling (Aspenström, 1999; Greenberg and Hatini, 2011; Hall, 2012; Cook et al., 2014). Rho1, Cdc42, and Rac (with three fly paralogs Rac1,

[1]Department of Cell and Systems Biology, University of Toronto, Toronto, ON, Canada; [2]Department of Genetics, Harvard Medical School, Boston, MA; [3]Howard Hughes Medical Institute, Harvard Medical School, Boston, MA; [4]RIKEN Center for Biosystems Dynamics Research, Minatojima-minamimachi, Kobe, Japan.

*J.T. Silver, F. Wirtz-Peitz, S. Simões, and M. Pellikka contributed equally to this paper; Correspondence to Ulrich Tepass: u.tepass@utoronto.ca; Norbert Perrimon: perrimon@receptor.med.harvard.edu; D. Yan's present address is Shanghai Institute of Plant Physiology and Ecology, Chinese Academy of Sciences, Shanghai, China.

Rac2, and Mtl) are maternally provided to the embryo (Magie et al., 1999; Genova et al., 2000; Hakeda-Suzuki et al., 2002). These Rho GTPases play multiple essential roles in embryogenesis through their contributions to epithelial polarity, cell movements such as mesoderm invagination, germband extension, dorsal closure, and wound repair, among other processes (Harden, 2002; Mack and Georgiou, 2014; Verboon and Parkhurst, 2015). However, how RhoGTPases are regulated in development through the spatial and temporal engagement of GEFs and GAPs still remains largely unexplored.

Here, we characterize a *Drosophila* RhoGEF, Cysts (Cyst). Cyst is the single orthologue of a group of four mammalian paralog GEFs characterized by the presence of a RhoGEF or Dbl homology–pleckstrin homology (DH-PH) domain: p114RhoGEF, p190RhoGEF, AKAP-13, and GEF-H1 (McCormack et al., 2013; Cook et al., 2014; Ngok et al., 2014). Tissue culture studies have shown that p114RhoGEF (ARHGEF18 in humans) links the epithelial polarity machinery with the actomyosin cytoskeleton. p114RhoGEF interacts with proteins of the apical Par and Crb polarity complexes and activates RhoA in support of actomyosin organization, apical constriction, and junction assembly (Nakajima and Tanoue, 2010, 2011, 2012; Terry et al., 2011; Loie et al., 2015; Acharya et al., 2018). Our work indicates that Cyst is a key RhoGEF in the *Drosophila* embryo that activates Rho1 and consequently myosin II at AJs. We conclude that Cyst is a crucial component of the apical polarity protein network that couples apical polarity to the junctional Rho1-myosin pathway, supporting AJ stability and epithelial integrity.

Results

Cyst is an apical epithelial polarity protein required for AJ stability during gastrulation

Maternal knockdown of *CG10188* caused an embryonic lethal phenotype characterized by the formation of many small epithelial vesicles or cysts instead of a large continuous epithelial sheet. We named *CG10188* therefore *cysts* (*cyst*; Fig. 1 C). These *cyst* RNAi embryos also develop larger patches of continuous epidermis displayed as shields of cuticle (Fig. 1 C). *cyst* RNAi embryos were rescued to adulthood by a Cyst[R] transgene, containing a *cyst* genomic sequence immune to *cyst* RNAi without altering the encoded protein sequence (Fig. 1 A). We also noted that overexpression of Cyst led to embryonic lethality, with embryos displaying severe defects in head morphogenesis (Fig. 1 F). These results identify Cyst as an essential factor for maintaining epithelial integrity in the *Drosophila* embryo.

We generated a *cyst* deletion mutation (*cyst¹*) with CRISPR/Cas9 technology that removes most of the *cyst* coding sequence including the DH (RhoGEF) and PH domains and the entire C-terminal part of the protein (Fig. 1 A). Zygotic *cyst¹* mutant animals were not embryonic lethal and died at later stages of development. In contrast, embryos derived from *cyst¹* mutant germline clones and crossed to *cyst¹*/+ showed two phenotypes. One half of embryos showed a prominent embryonic phenotype similar to *cyst* RNAi embryos (referred to as *cyst¹*(M/Z) embryos here), characterized by the presence of a large number of epithelial vesicles and shields of cuticle of various sizes (Fig. 1, D

and E). The other half of animals were not embryonic lethal, suggesting that maternal depletion of Cyst can be compensated for by expression of one zygotic copy of *cyst*. The *cyst* phenotype is reminiscent of the *crb* mutant phenotype (Fig. 1 G; Tepass et al., 1990; Tepaß and Knust, 1990; Tepass and Knust, 1993) or the phenotype caused by depletion of other apical polarity proteins or AJ proteins such as DE-cadherin (DEcad; Tepass et al., 1996; Uemura et al., 1996). Whereas most *crb* mutant embryos showed only cuticle vesicles, all *cyst¹*(M/Z) or *cyst* RNAi embryos showed cuticle shields in addition to vesicles, suggesting that the *cyst*-null phenotype is qualitatively similar but somewhat weaker than the *crb*-null phenotype.

A *crb*-like phenotype has been documented for only a small number of genes that encode apical polarity proteins such as *crb* and *stardust* (*sdt*), or genes encoding AJ proteins such as *bazooka* (*baz*), *shotgun* (encoding DEcad), or *armadillo* (*arm*; *Drosophila* β-catenin; Tepass et al., 1990, 1996; Tepaß and Knust, 1990; Tepass and Knust, 1993; Cox et al., 1996; Uemura et al., 1996; Bilder et al., 2003; Tanentzapf and Tepass, 2003). In contrast, genes encoding basolateral polarity proteins such as *scribble* (*scrib*) or *yurt* (*yrt*) have different mutant phenotypes and do not display epithelial cysts with inward-facing apical lumina. Instead, these mutants display clusters of epithelial cells with enlarged apical membranes so the cuticle appears as a series of bubbles (Bilder and Perrimon, 2000; Bilder et al., 2003; Tanentzapf and Tepass, 2003; Laprise et al., 2006, 2009). The cuticle defects observed in *cyst*-compromised embryos therefore strongly suggest that Cyst is a new component of the apical polarity machinery.

The development of a *crb*-like phenotype was described in detail and entails the loss of polarity and AJ fragmentation during gastrulation (stages 8–11; Tepass et al., 1990; Tepaß and Knust, 1990; Grawe et al., 1996; Tepass, 1996). Subsequently, these embryos show enhanced programmed cell death elicited by activation of the JNK signaling pathway (Kolahgar et al., 2011). Epithelial cells that survive form cysts that show normal epithelial polarity with an inward-facing lumen into which cuticle is secreted (Tanentzapf and Tepass, 2003). To determine whether a similar sequence of events can be found in *cyst*-compromised embryos, we examined the development of *cyst* embryos by live imaging, monitoring the AJ marker DEcad::GFP (Fig. 2) and assessing the distribution of apical (Crb and aPKC), junctional (Arm), and basolateral (Yrt) polarity markers (Figs. 3 and S1). These observations showed progressive AJ fragmentation during gastrulation until many cells, in particular in the ventral ectoderm, had lost AJs (Fig. 2, A and B). Other cells showed focal concentrations of DEcad, suggesting the beginning of cyst formation (Fig. 2 C). Formation of epithelial cysts is first seen at the end of gastrulation in stage-11 embryos and can be followed throughout the rest of development (Figs. 3 and S1). These cysts showed normal polarized distribution of Crb, aPKC, Arm, and Yrt (Figs. 3 and S1). Collectively, these findings indicate that Cyst function is closely related to apical and/or junctional epithelial polarity regulators.

A key feature of the machinery that regulates epithelial polarity is the negative feedback between apical and basolateral polarity proteins (Benton and St Johnston, 2003; Bilder et al.,
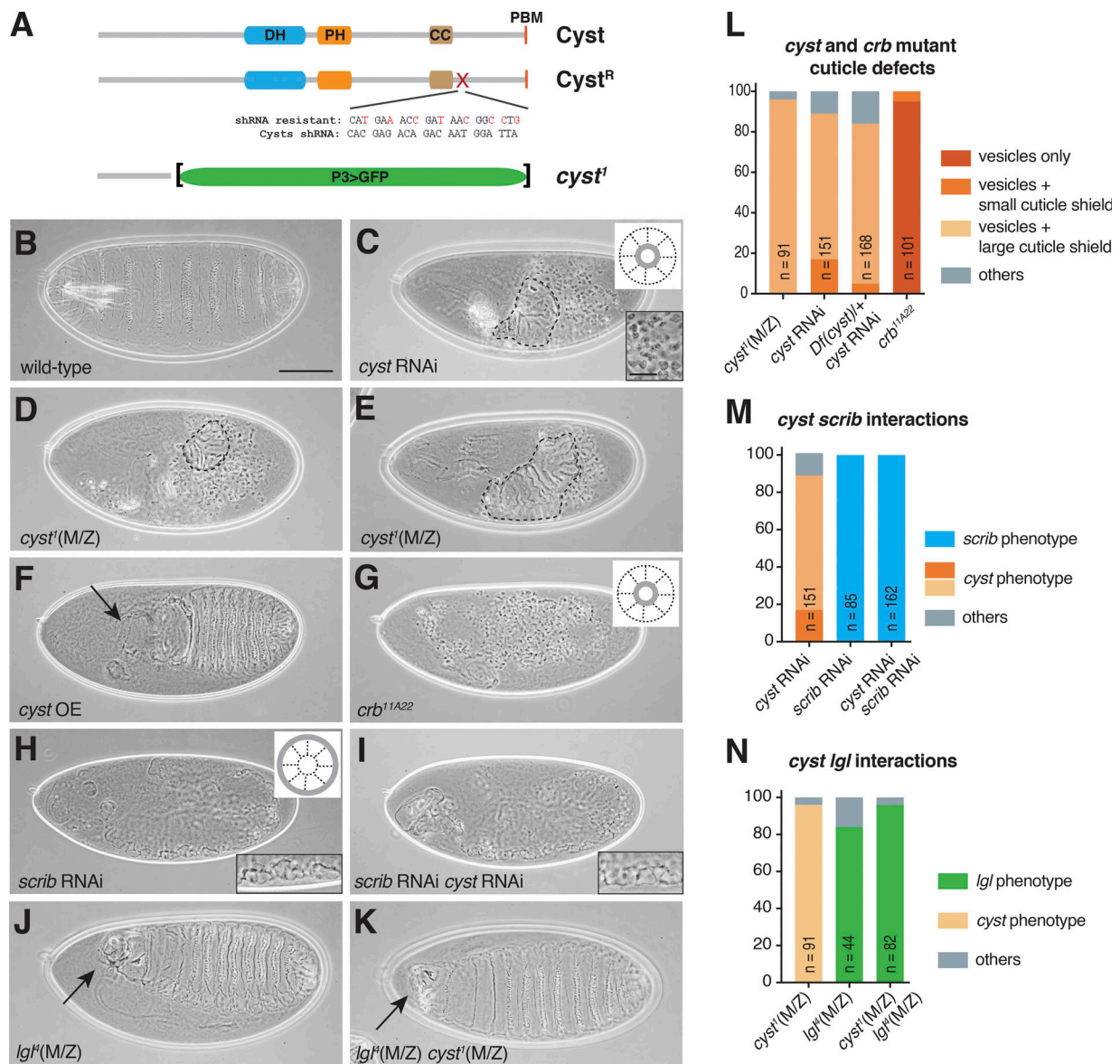
Figure 1. **Cyst maintains epithelial polarity. (A)** Schematic of Cyst, Cyst^R (shRNA resistant), and cyst^1. Cyst^R is encoded by a cyst genomic sequence including the endogenous promotor that has been mutagenized to render it immune to cyst shRNA. cyst^1 is a genomic deletion in which cyst sequence has been replaced by GFP driven by the P3 promoter. **(B–K)** Cuticles of embryos of the indicated genotypes. cyst RNAi (C and I) and scrib RNAi (H and I) embryos were derived from mothers expressing shRNAs with mat-Gal4. cyst^1(M/Z) and lgl^4(M/Z) are cyst^1 mutant (D, E, and K) and/or lgl^4 mutant (J and K) germline clones. cyst OE (overexpression), mat-Gal4 UAS-cyst^R embryo (F, n = 30). crb^{11A22}, crb-null mutant embryo (G). Inset in C shows cuticle vesicles/cysts. The schematics in C and G illustrate the cellular organization of epithelial cysts in cyst- and crb-compromised embryos with cuticle highlighted as gray lines. Insets in H and I show the bubbly cuticle defects typical for scrib-depleted embryos. The schematic in H illustrates the cellular organization of bubbles in scrib-compromised embryos with cuticle highlighted as gray line. Dashed lines encircle cuticle shields. Arrows point to head defects. Scale bars, 100 µm; insets, 25 µm. **(L–N)** Quantification of cuticle defects of indicated genotypes.

2003; Tanentzapf and Tepass, 2003; Laprise et al., 2009; Chartier et al., 2011; Fletcher et al., 2012; Gamblin et al., 2014). This mutual antagonism can be revealed through double-mutant analysis. For example, double mutants of crb and the basolateral polarity gene scrib or of sdt and the basolateral polarity gene lethal giant larvae (lgl) show a striking suppression of the crb or sdt mutant defects and display a scrib or lgl mutant phenotype, respectively (Bilder et al., 2003; Tanentzapf and Tepass, 2003). To reveal whether cyst behaves like crb or sdt in these tests, we generated embryos compromised for cyst and scrib or cyst and lgl

(Fig. 1, H–K, M, and N). Maternal depletion of scrib with RNAi caused a strong loss-of-function phenotype characterized by epidermal cell clusters surrounded by cuticle (Fig. 1 H; Bilder et al., 2003; Tanentzapf and Tepass, 2003), whereas lgl^4(M/Z) embryos displayed a weaker phenotype with defects in head morphogenesis. scrib RNAi fully suppressed the cyst RNAi phenotype, and lgl^4(M/Z) fully suppressed the cyst^1(M/Z) phenotype, with double mutants showing phenotypes indistinguishable from scrib RNAi or lgl^4(M/Z) alone (Fig. 1, I, M, K, and N). Taken together, our analyses suggest that Cyst is a new key component
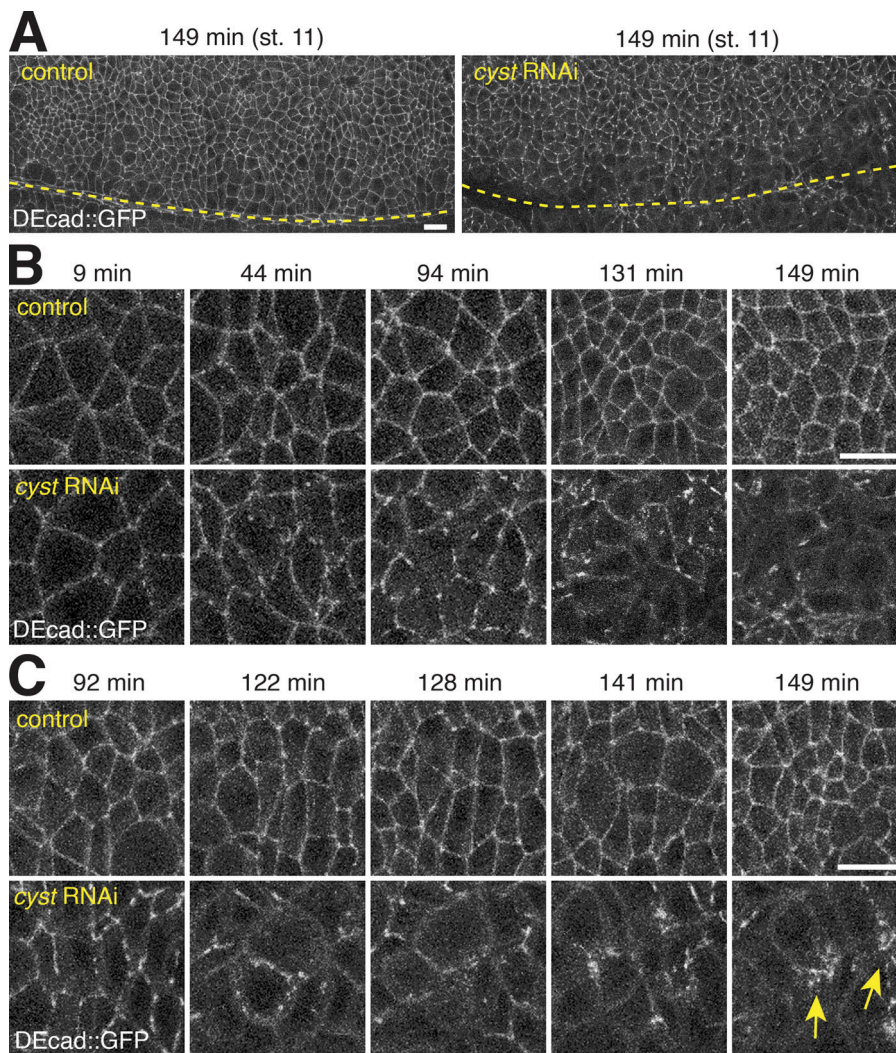
A 149 min (st. 11) 149 min (st. 11)

control cyst RNAi

DEcad::GFP

B 9 min 44 min 94 min 131 min 149 min

control

cyst RNAi

DEcad::GFP

C 92 min 122 min 128 min 141 min 149 min

control

cyst RNAi

DEcad::GFP

Figure 2. **Cyst is required for AJ integrity.** Z-projections (9.5 µm) taken from live control (n = 3) or cyst RNAi (n = 3) embryos expressing DEcad::GFP controlled by its endogenous promoter (see Videos 1 and 2). Times indicate minutes after onset of germband extension. Scale bars, 10 µm. **(A)** Ventral view of the ectoderm at stage 11 showing a loss of AJs in cells adjacent to the ventral midline (dashed line) in a cyst RNAi embryo. **(B)** Ventral ectoderm cells at the indicated time points showing the increasing fragmentation and loss of AJs in a cyst RNAi embryo. **(C)** Ventral ectoderm cells at the indicated time points showing clustering of AJ material in a cyst RNAi embryo (arrows).

of the apical polarity machinery that acts during gastrulation to maintain junctional and epithelial integrity in fly embryos.

Cyst regulates planar epithelial organization in the early embryo

To further assess the role of Cyst in the early embryo, we analyzed the lateral ectoderm at the onset of germband extension, when circumferential AJs form. At this stage, DEcad, Baz, and other AJ proteins become enriched at the apico-lateral boundary but also acquire a planar polarized distribution to the dorsal and ventral edges of the apico-lateral domain (Zallen and Wieschaus, 2004). Disrupted planar polarization, with Baz hyperpolarizing as prominent, single foci along cell edges, has been observed when actin is reduced or in embryos with abnormal activity of polarity proteins including aPKC, Par1, and Crb (Harris and Peifer, 2007; Jiang et al., 2015; Vichas et al., 2015). This tissue thus provides a context to examine whether Cyst cooperates with polarity proteins in the initial formation of a normal circumferential AJ belt.

We found that cyst depletion by maternal expression of shRNA alone had minimal effects on Baz distribution. However, further depletion of cyst by maternal heterozygosity for a

deletion uncovering cyst (Df(cyst) = Df(2L)BSC301) produced Baz hyperpolarization in contrast to control (mCherry shRNA) or Df(cyst)/+ alone (Fig. 4, A and B). To test if Baz hyperpolarization was subject to regulation by aPKC, we analyzed cyst RNAi; Df(cyst)/+ embryos derived from mothers heterozygous for a null aPKC allele and discovered even greater Baz hyperpolarization, whereas Df(cyst) apkc/+ control embryos were normal (Fig. 4, A and B). As compromising the Cdc42-binding region of Par6 disrupts the cortical localization of the Par6/aPKC complex (Hutterer et al., 2004), we investigated whether the misregulation of Baz by cyst depletion could be explained by a loss of aPKC from the apical domain. However, cyst loss-of-function embryos displayed no detectable effects on aPKC localization when the blastoderm was fully formed and before the germband started to extend (Fig. 4 C) or on aPKC levels around the margins of the apical domain (Fig. 4, C and D). As an alternative possibility, we examined if disruption of F-actin could explain the observed hyperpolarization of Baz. Treatment of embryos with cytochalasin D resulted in Baz hyperpolarization (Fig. 4 E), with no apparent effect on aPKC levels at the apico-lateral membrane (Fig. 4 F), mimicking the effects of cyst loss of function. These results indicate that Cyst contributes to the initial formation of a
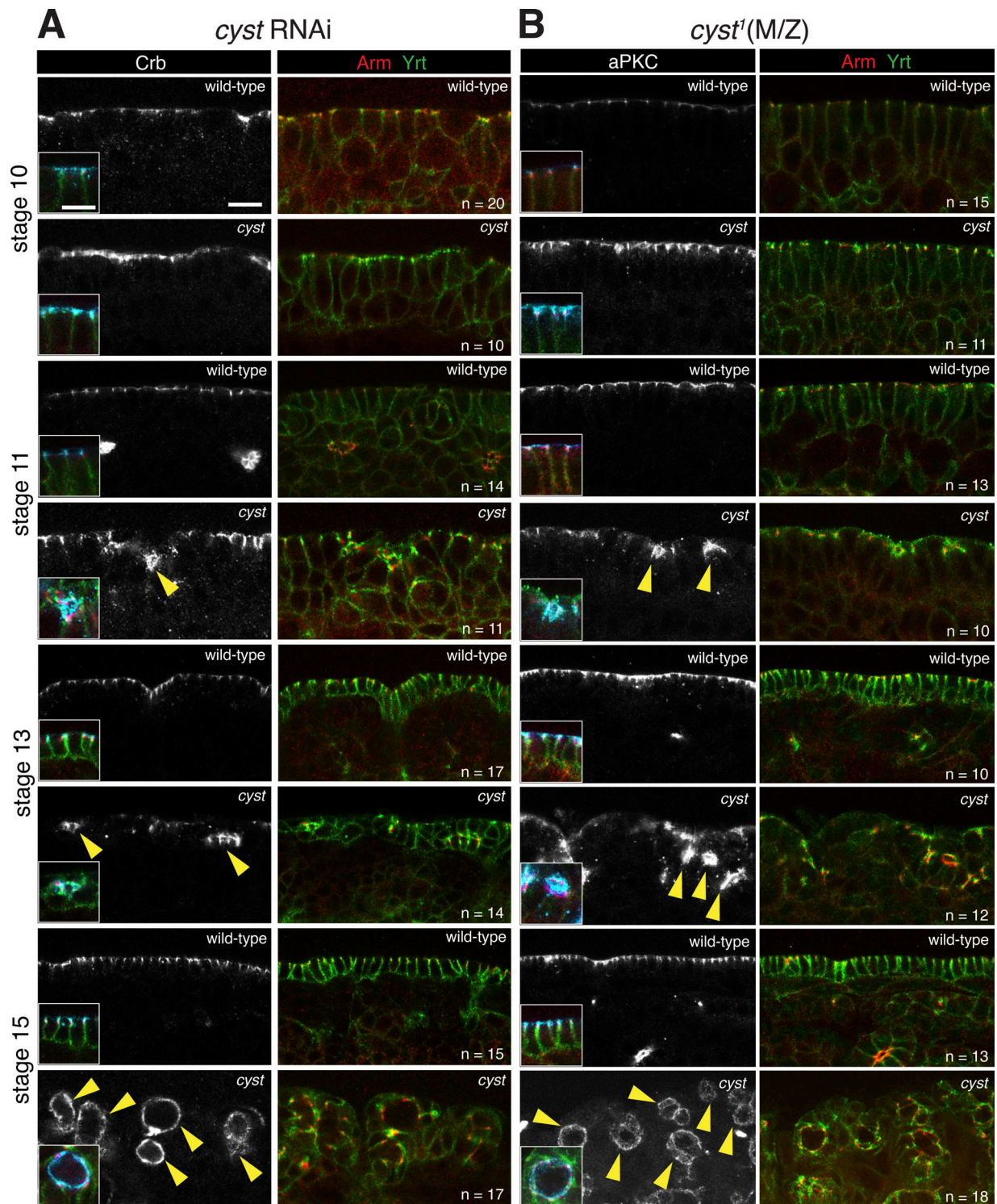
Silver et al.
RhoGEF Cysts links polarity to junctional myosin

Journal of Cell Biology 3400
https://doi.org/10.1083/jcb.201807106

Figure 3. **Epithelial cysts in *cyst*-compromised embryos maintain epithelial polarity. (A and B)** Staining of *cyst* RNAi (A) and *cyst¹*(M/Z) (B) embryos compared with wild-type controls for the apical markers Crb and aPKC, the junctional marker Arm, and the basolateral marker Yrt. All panels show side views of the ectoderm or epidermis at the indicated stages. Epithelial cysts in *cyst*-compromised embryos are evident in stage-11, -13, and -15 embryos (arrowheads) but not at stage 10. Markers show normal subcellular distributions of apical markers in cysts, facing the lumen where cuticle will be secreted (see Fig. 1, C–E). Insets show triple-labeled cells with Crb (A) or aPKC (B) shown in blue. *n* = number of embryos analyzed. Scale bars, 10 μm; insets, 5 μm.

normal circumferential AJ belt. Cyst appears to act by regulating the actin cytoskeleton, either downstream or in parallel with an aPKC-dependent mechanism.

Cyst localizes to the apico-lateral cortex
The impact of Cyst on AJs suggests that it may localize to the apico-lateral cortex to exert its function. We examined the
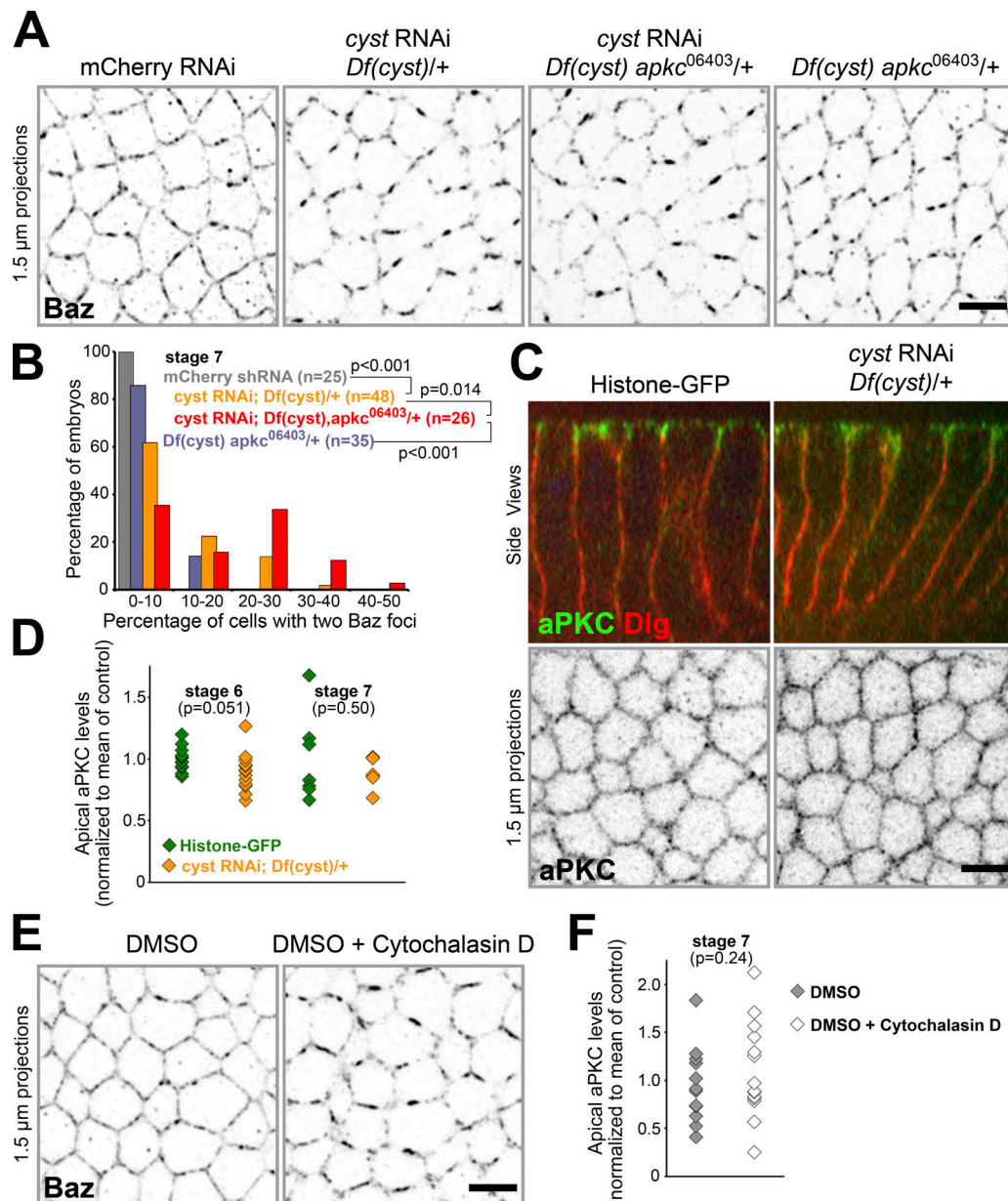
Silver et al.
RhoGEF Cysts links polarity to junctional myosin

Journal of Cell Biology 3401
https://doi.org/10.1083/jcb.201807106

Figure 4. **Cyst contributes to the initial formation of an AJ belt. (A)** Localization of Baz in the apico-lateral domain of the lateral ectoderm at the onset of germband extension. Reduction of *cyst* expression through the combination of maternal shRNA (using MTD-GAL4) and maternal heterozygosity for *Df(cyst)* resulted in Baz planar hyperpolarization into foci. Additional incorporation of maternal heterozygosity for a null *apkc* allele enhanced the hyperpolarization of Baz. A control shRNA, or the combined heterozygosity of *Df(cyst)* and *apkc*, had no apparent effects. Scale bar, 5 μm. **(B)** Quantification of the data shown in A. *n* values represent embryo numbers. **(C)** Side views (top) and apical domain surface projections (bottom) showing indistinguishable apical polarization and apical levels of aPKC with Cyst depletion versus controls at the onset of germband extension. Dlg labels the lateral domain. Scale bar, 5 μm. **(D)** Quantification of the data shown in C. Each point is a quantification of one embryo. **(E)** Cytochalasin D produces Baz hyperpolarization at the onset of germband extension, in contrast to carrier DMSO control. Scale bar, 5 μm. **(F)** Cytochalasin D has no apparent effect on apical aPKC levels at the onset of germband extension. Each point is a quantification of one embryo. For B, D, and F, pairwise comparisons were done using Student's *t* test in Microsoft Excel. Data presented as mean + SEM.

distribution of an N-terminally GFP-tagged isoform of Cyst (GFP::Cyst^R) expressed under the *cyst* endogenous promoter in live embryos. GFP::Cyst^R was enriched at the apico-lateral cortex (Fig. 5 A). GFP::Cyst^R was barely detectable at stage 6, increased at the cortex from stage 8 to mid-embryogenesis (stage 14), and decreased at later stages (Fig. 5 B). These findings suggest that Cyst is enriched at AJs or their immediate vicinity from the

onset of germband extension (stage 6/7) and throughout organogenesis.

The RhoGEF domain and the C-terminal region are essential for Cyst function

shRNA-resistant genomic structure–function constructs were tested for their ability to rescue the embryonic lethality and
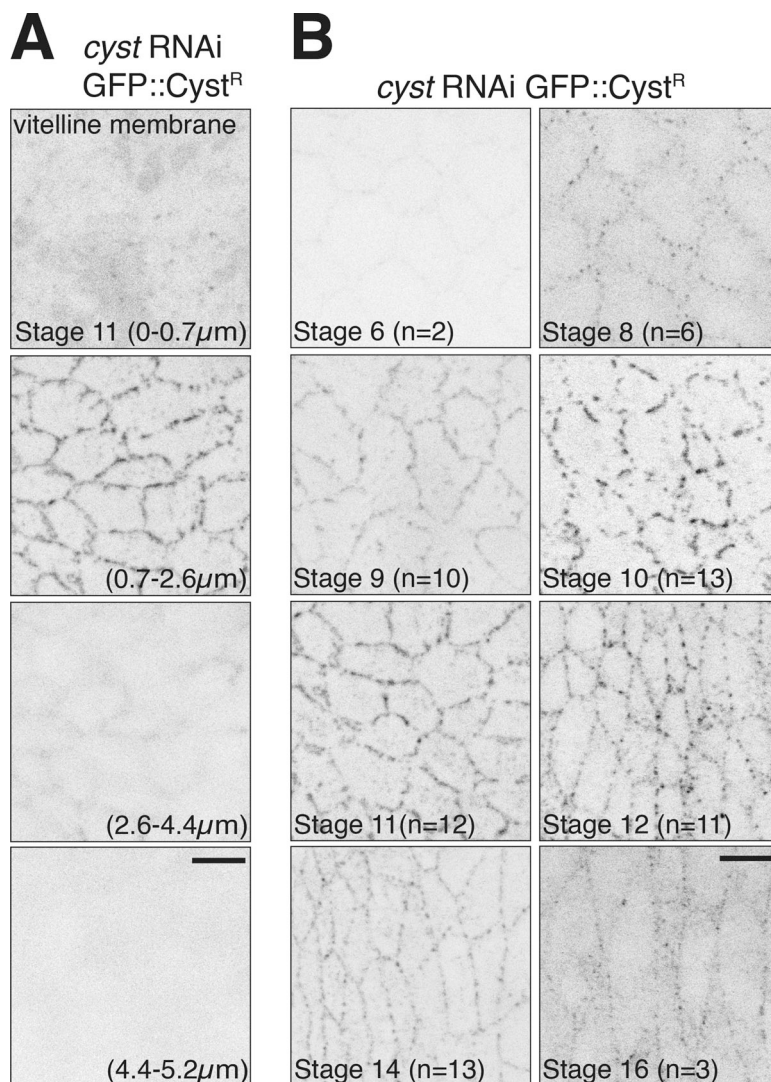
A *cyst* RNAi GFP::Cyst^R

B *cyst* RNAi GFP::Cyst^R

Figure 5. **Cyst localizes to the apico-lateral cortex of epithelial cells. (A)** Four z-projections of the ventral ectoderm (0.37-μm step size) showing 5.2-μm depth from a live *cyst* RNAi embryo rescued by GFP::Cyst^R. GFP::Cyst^R is enriched at the apico-lateral cortex immediately below the vitelline membrane (0.0–0.7 μm). Scale bar, 5 μm. **(B)** Z-projections of junctional region (0.37-μm step size) of the ventral ectoderm or epidermis from live *cyst* RNAi embryos rescued by GFP::Cyst^R of the indicated stages. Scale bar, 5 μm.

phenotype of *cyst* RNAi embryos. Cyst RNAi embryos are embryonic lethal and display a loss of epithelial integrity (Figs. 1 and 3). As expected, a construct lacking the DH-PH domain of Cyst (Cyst^RΔDH-PH::GFP) did not rescue *cyst* RNAi embryos, in contrast to control constructs (Cyst^R, Cyst^R::GFP, GFP::Cyst^R; Fig. 6), indicating that the RhoGEF domain of Cyst is essential for epithelial integrity. Also, a construct lacking the C-terminal region of Cyst (Cyst^RΔC::GFP) did not rescue the *cyst* RNAi phenotype (Fig. 6). In contrast, *cyst* RNAi embryos expressing GFP::Cyst^RΔPBM, which lacks the C-terminal predicted PDZ domain binding motif (PBM), were viable, indicating that the Cyst C-terminal region, but not the PBM, is essential for function, consistent with our finding that Cyst interacts with PDZ domain–containing proteins Baz and Patj independent of its PBM (see below). Expression of a construct lacking the Cyst N-terminus (GFP::Cyst^RΔN) rescued the lethality of most *cyst* shRNA embryos (Fig. 6, A and B), with dead embryos displaying a normal cuticle, indicating that the N-terminal region of Cyst is dispensable for most Cyst activity. As Cyst contains a putative aPKC phosphorylation site in its N-terminal region at S320 (Wang et al., 2012a), we asked whether aPKC phosphorylation of

Cyst could potentially modify its activity. However, non-phosphorylatable and phosphomimetic isoforms of Cyst (GFP::Cyst^RS320A and GFP::Cyst^RS320E) fully rescued *cyst* shRNA embryos (Fig. 6). Taken together, our analysis shows that the RhoGEF activity and the coiled-coil domain (CC) containing C-terminal region of Cyst are essential for its function.

Apical recruitment of Cyst requires physical interaction with the Crb complex and Baz/Par3

Previous work indicated that mammalian p114RhoGEF forms complexes with Lulu2 (also known as EPB41L4B, one of two mammalian homologues of *Drosophila* Yrt), Patj, and Par3 (Nakajima and Tanoue, 2011). To probe for similar interactions among *Drosophila* proteins, we first asked whether the Crb complex, which includes Patj, and Baz are required for Cyst recruitment to the apico-lateral cortex. We injected GFP::Cyst-expressing embryos with double-stranded RNA (dsRNA) against *crb* or *baz*. In both cases, GFP::Cyst was lost from the cortex (Fig. 7 A).

To probe for physical interactions, we coexpressed various GFP-tagged fragments of Cyst with FLAG-tagged Baz or Patj (Baz::FLAG or Patj::FLAG) in HEK293T cells. We found that
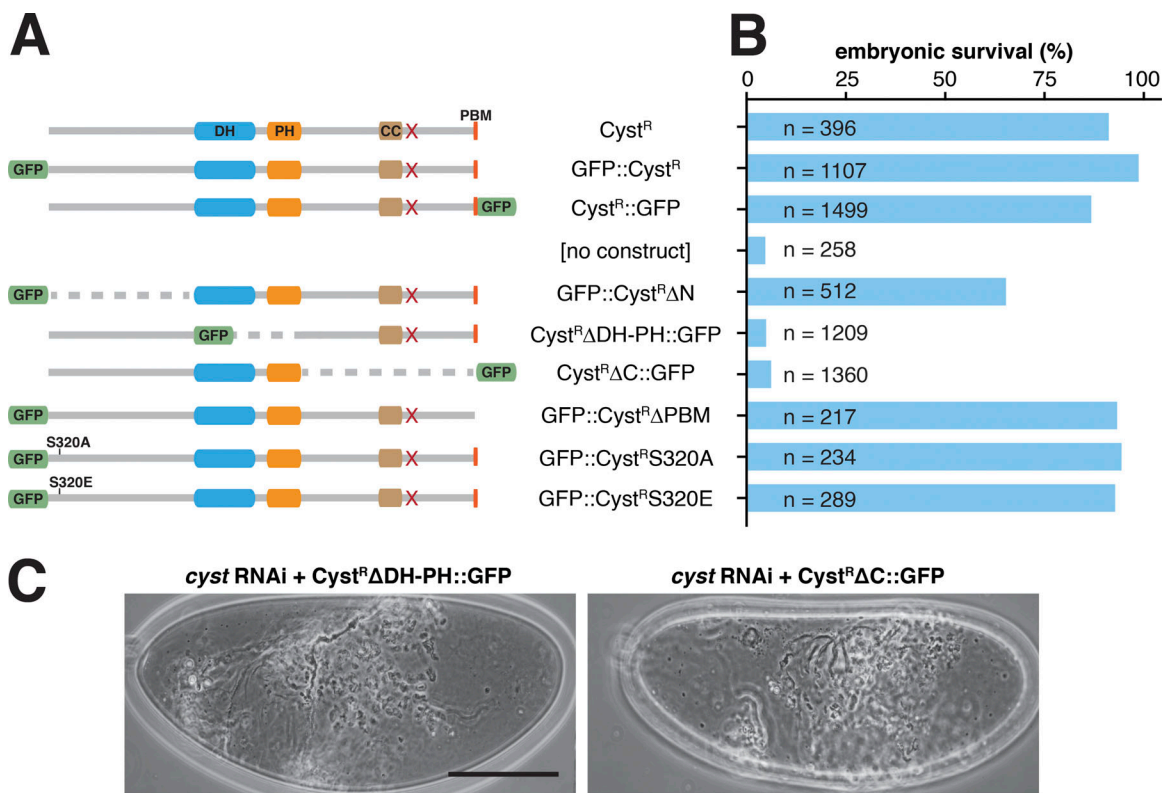
Figure 6. **Cyst contains essential RhoGEF and C-terminal regions. (A)** Schematic of Cyst[R] GFP-tagged structure–function constructs. Constructs were generated from the *cyst* genomic region, expressed under the endogenous promoter, and are immune to *cyst* shRNA (red cross; see Fig. 1 A). GFP replaces deleted regions (dashed lines). **(B)** Quantification of embryonic survival when Cyst isoforms were expressed in a *cyst* RNAi background. Cyst[R]ΔN partially rescues *cyst* RNAi embryos (68% embryonic viable). *n* = number of fertilized eggs analyzed. Survival was scored by subtracting the number of hatched larvae from total number of (fertilized) embryos counted. Whether eggs were fertilized or not was determined in cuticle preparations. **(C)** Embryo cuticles of the indicated genotypes showing that Cyst[R]ΔDH-PH and Cyst[R]ΔC fail to rescue the *cyst* RNAi phenotype. Scale bar, 100 µm.

GFP::Cyst and GFP::Cyst-C coimmunoprecipitated with Baz::FLAG or Patj::FLAG, with the interaction between Cyst-C and Patj appearing particularly robust (Fig. 7, B and D). Interestingly, GFP::CystΔPBM also formed Baz::FLAG- or Patj::FLAG-containing complexes, suggesting that the interaction between Cyst and Baz or Patj takes place in the C-terminal region of Cyst but does not require the Cyst PBM. To further assess whether Cyst and Baz can interact, we coexpressed FLAG-tagged versions of Cyst N, DH-PH, and C-terminal regions with GFP-tagged Par3 (GFP::Par3) in HeLa cells. We found that FLAG::Cyst-C and GFP::Par3 appeared to coaggregate in puncta (Fig. S2). These findings suggest that *Drosophila* Cyst undergoes molecular interactions with the Crb complex and Baz to support its apico-lateral localization. In contrast to findings in mammalian cells (Nakajima and Tanoue, 2011; Loie et al., 2015), we did not detect molecular interactions between Yrt and Cyst. This correlates with the observation that Yrt acts as a basolateral polarity protein in early *Drosophila* embryos and that the *yrt* mutant phenotype is different from the *cyst* phenotype (Laprise et al., 2006, 2009).

To further explore the function of the C-terminal region of Cyst, which is crucial for Cyst function, we coexpressed FLAG::Cyst-C with various GFP-tagged fragments of Cyst in HEK293T cells. We detected binding of GFP::Cyst, GFP::CystΔPBM, and GFP::Cyst-C to FLAG::Cyst-C (Fig. 7, C and D).

These constructs all contain the Cyst CC, which facilitates oligomerization in some CC proteins (Schultz et al., 1998; Letunic et al., 2015). Taken together, our data support the view that Cyst is directed to the apico-lateral cortex through a multifaceted mechanism, potentially involving Cyst oligomerization, and redundant and/or parallel interactions between Cyst C-terminal region and Baz and the Crb complex.

Cyst targets Rho1

RhoGEF domains often show specificity for Rho, Rac, or Cdc42, although there are examples of promiscuity (McCormack et al., 2013; Ngok et al., 2014). Phylogenetic analysis suggests that Cyst is the single orthologue of a group of four mammalian RhoGEFs that target RhoA in cell culture. To ask whether Cyst targets Rho1 in vivo, we assayed the activity of two probes that are thought to preferentially bind to Rho1-GTP: Anillin-RBD::GFP (Munjal et al., 2015; Fig. 8, A and B) and PKNG58A::GFP (Simões et al., 2014; Fig. S3). The junctional localization of both probes was reduced by ~30–60% in *cyst*-compromised embryos compared with controls.

To further assess interactions between Cyst and Rho1, we asked whether Cyst activates Rho1 in cell culture. We coexpressed FLAG-tagged versions of *Drosophila* Rho1, Rac1, and Cdc42 along with the DH-PH domain of Cyst fused to GFP
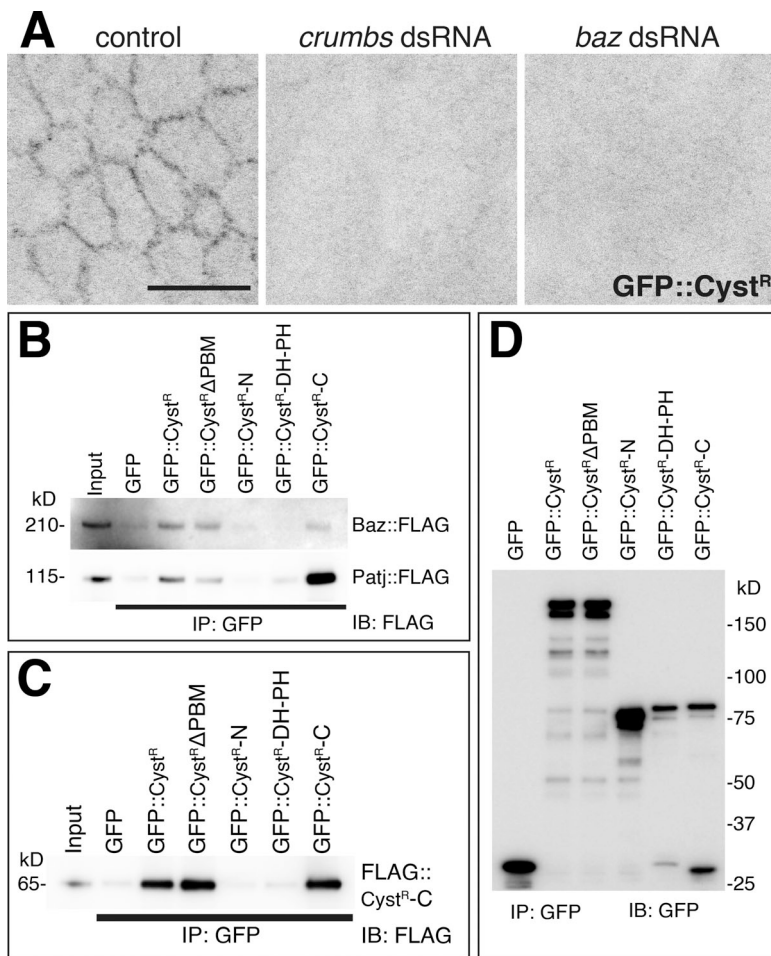
Figure 7. **Cyst physically interacts with Baz and the Crb complex.** **(A)** Z-projections taken from live stage-9 embryo expressing GFP::Cyst^R. Embryos have been injected with dsRNAs against *crb* or *baz* ($n = 40$ each). GFP::Cyst^R is lost from the cortex in knockdown embryos. Scale bar, 10 µm. **(B)** Immunoprecipitation (IP) with anti-GFP followed by immunoblot (IB) with anti-FLAG. Cyst constructs were coexpressed with Baz::FLAG and Patj::FLAG in HEK293T cells. Input shows Baz::FLAG and Patj::FLAG bands. GFP::Cyst^R and GFP::Cyst^{R}ΔPBM formed Baz::FLAG- or Patj::FLAG-containing complexes. GFP::Cyst^R-C and Patj::FLAG formed a particularly strong complex. GFP::Cyst^R-C and Baz::FLAG formed a weak complex. **(C)** Immunoprecipitation with anti-GFP followed by immunoblot with anti-FLAG. A FLAG-tagged version of Cyst C-terminal region (FLAG::Cyst^R-C) was coexpressed with various GFP-tagged fragments of Cyst (or GFP as a control) in HEK293T cells. Input shows FLAG::Cyst^R-C. GFP::Cyst^R, GFP::Cyst^{R}ΔPBM, and GFP::Cyst^R-C formed FLAG:: Cyst^R-C–containing complexes. **(D)** Controls for B and C. Immunoprecipitation with anti-GFP followed by immunoblot with anti-GFP. All GFP-tagged constructs are expressed.

(Cyst-DH-PH::GFP) or N or C fragments (GFP::Cyst-N or GFP::Cyst-C) as controls in HEK293T cells (Fig. 8 C). Immunoprecipitation of the GTPases was followed by direct analysis of absolute levels of associated GTP and GDP by liquid chromatography/tandem mass spectrometry (LC-MS/MS). Coexpression of Cyst-DH-PH::GFP with Rho1 showed a twofold increase in Rho1-associated GTP as normalized to the levels seen with GFP::Cyst-N (Fig. 8 D). As a positive control, the DH-PH domain of LARG, a known mammalian RhoA-GEF (Cook et al., 2014), showed a level of Rho1 GTP loading comparable to that of Cyst-DH-PH::GFP (Fig. 8 E). These data are consistent with our observation that the expression of Cyst-DH-PH::GFP, but not GFP::Cyst-N or GFP::Cyst-C, produces dorsal ruffling and stress fiber formation in HeLa cells (Fig. S2), a phenotype reminiscent of RhoA activation in fibroblasts (Hall, 2012; Hanna and El-Sibai, 2013). We detected a 1.5-fold relative increase in GTP-associated Rac1. However, the level of Rac1 targeting by Cyst-DH-PH::GFP was less than that seen for an active version of the Rac-specific GEF STEF-ΔN (Matsuo et al., 2003), which acted as a positive control (Fig. 8, D and E). No detectable activation of Cdc42 was found.

Finally, we tested the ability of Cyst to suppress the effects of dominant-negative (DN) isoforms of Rho1 (Strutt et al., 1997), Rac1, and Cdc42 (Luo et al., 1994). Expression of any DN GTPases produced a prominent cuticle phenotype. This is presumably due to the sequestration of GEFs preventing activation of Rho,

Rac, or Cdc42. We hypothesized therefore that overexpression of a GEF could rescue the effects of a DN GTPase if active levels of its target GTPase are restored. We coexpressed upstream activation sequence (UAS)–controlled Cyst^R or the N-terminal region of Cyst (Cyst^R-N) as a negative control, with DN versions of Rho1, Rac1, or Cdc42. Overexpression of Cyst^R produced a cuticle that is intact, with the exception of a head defect (Fig. 1 F). We found that coexpression of Cyst^R with DN-Rho1 partially rescued the DN-Rho1 cuticle defects (Fig. S3), whereas no rescue was observed with Cyst^R-N. In contrast, expression of Cyst^R did not ameliorate the phenotypes resulting of expression of the DN forms of Rac1 or Cdc42. Collectively, our genetic and biochemical data support the conclusion that Cyst acts on Rho1.

Cyst and Crb are required for normal myosin II enrichment at AJs

AJ stability is tightly connected to actomyosin dynamics (Lecuit and Yap, 2015). To ask whether Cyst plays a role in actomyosin dynamics at AJs, we examined the distribution of myosin II by following fluorescent protein–tagged regulatory light chain of nonmuscle myosin II (Spaghetti Squash; Royou et al., 1999) in live embryos derived from *cyst* RNAi *Df(cyst)*/+ mothers (Fig. 9, A, B, and D). In the ectoderm, myosin II is recruited to the apico-lateral cortex during stages 6 and 7, just before the onset of germband extension. Defects in myosin II
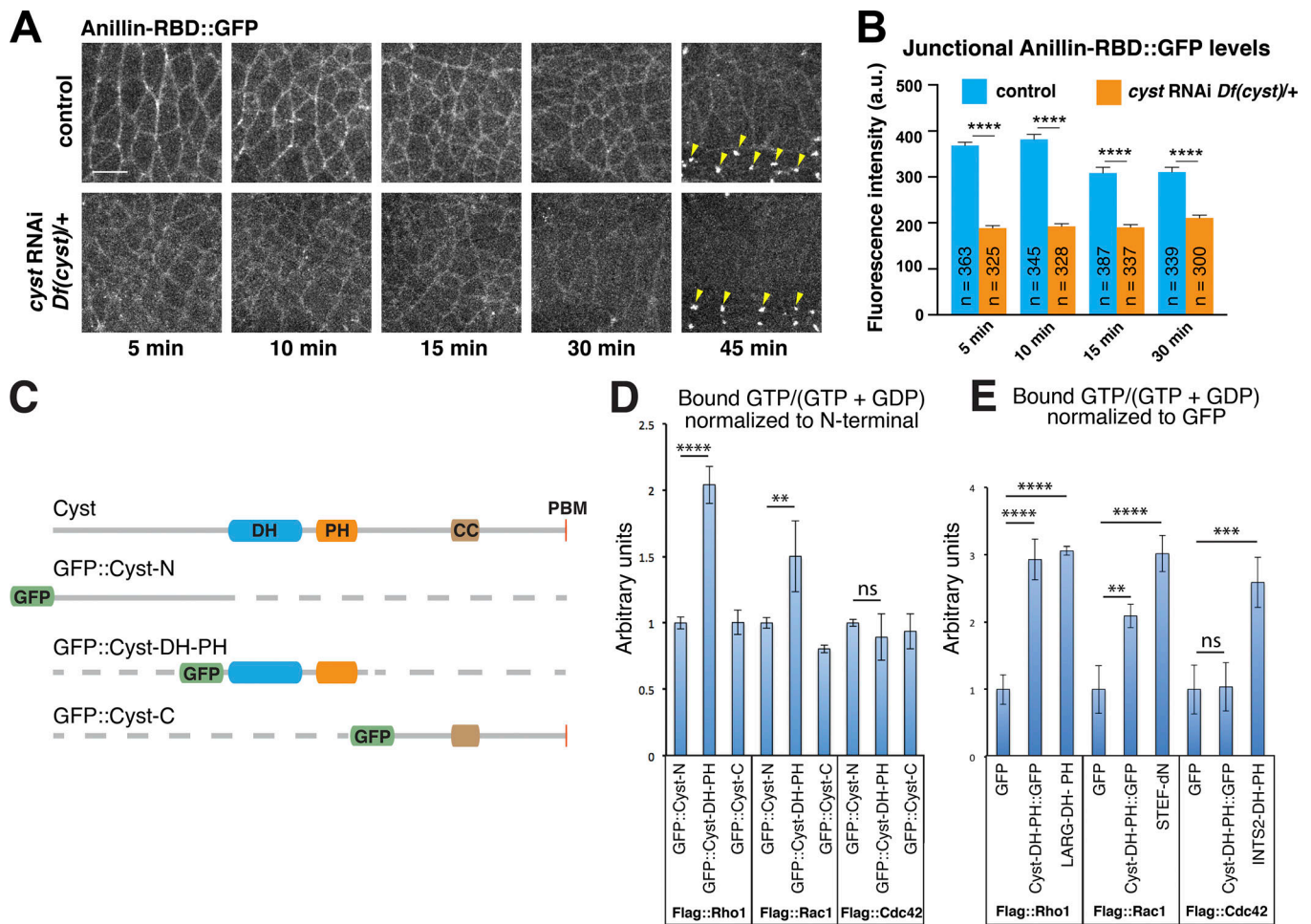
Figure 8. **Cyst preferentially targets Rho1. (A)** Stills of time-lapse videos (Videos 3 and 4) showing the Rho activity probe Anillin-RBD::GFP in a control and in an embryo derived from a *cyst* RNAi *Df(cysts)/+* mother. Time is minutes after the onset of germband extension. Junctional levels of Anillin-RBD:: GFP are reduced in *cyst*-depleted embryos. In ventral midline cells, the probe also accumulates in midbodies after cell division (arrowheads) in control and *cyst*-depleted embryos. Scale bar, 10 µm. **(B)** Quantification of junctional levels of Anillin-RBD::GFP in control and *cyst*-depleted embryos at the time points indicated in A. Quantifications at 45 min were not included, as the probe's junctional signal was undetectable in *cyst*-depleted embryos. Bars indicate mean ± SEM. *n* = number of cell edges analyzed in four embryos per condition. ****, From left to right: P = 1.5×10^{-60}, 8.3×10^{-42}, 1.2×10^{-9}, and 1.3×10^{-10} (Kolmogorov–Smirnov test). **(C)** Schematic of GFP-tagged fragments of Cyst used in D and E. **(D)** Activation of *Drosophila* Rho1, Rac1, or Cdc42 by the indicated fragments of Cyst protein depicted in C. GTPases were immunoprecipitated from HEK293T cells coexpressing the Cyst fragments. GTP and GDP were eluted and subsequently analyzed by LC-MS/MS. The absolute amounts of GTP and GDP are shown as a percentage normalized to coexpression with GFP::Cyst-N. GFP::Cyst-DH-PH showed a twofold relative increase in Rho1-associated GTP and a 1.5-fold relative increase in GTP-associated Rac1. No detectable activation of Cdc42 was found. GFP::Cyst-N and GFP::Cyst-C act as negative controls. *n* = 4 for all measurements. Data are presented as mean ± SD. ****, P < 0.0001; **, P < 0.01; ns, not significant (Student's *t* test). **(E)** Positive controls for D using mammalian GEF proteins. The DH-PH domain of LARG (LARG-DH-PH), an active version of STEF (STEF-ΔN), and the DH-PH domain of INTS2 (INTS2-DH-PH) are known to target Rho1, Rac1, and Cdc42, respectively. GFP::Cyst-DH-PH and LARG-DH-PH show comparable targeting of Rho1. GFP::Cyst-DH-PH targeting of Rac1 was less than that seen for STEF-ΔN. Values are normalized to GFP, which acts as a negative control. *n* = 4 for all measurements. Data are presented as mean ± SD. ****, P < 0.0001; ***, P < 0.001; **, P < 0.01; ns, not significant (Student's *t* test).

were noted from stage 7 onward, with junctional myosin levels reduced and less uniformly distributed around the apical cell perimeter. Interestingly, a similar reduction in junctional myosin was observed in *crb* RNAi embryos (Fig. 9, C and E). In contrast, medial myosin II levels behaved differently in Crb- and Cyst-depleted embryos as germband extension progressed. Whereas medial myosin II levels were enhanced in Crb-compromised embryos compared with controls, Cyst-depleted embryos showed a moderate reduction in medial myosin II (Fig. 9, D and E).

We also found that the loss of Cyst causes aberrant F-actin distribution and dynamics, as assayed by Utrophin::GFP (stage 11/12; Fig. S4 and Videos 9 and 10), including in small groups of cells that go on to form epithelial cysts. Moreover, high levels of F-actin were associated with apical protrusions, consistent with a loss of Rho activity and AJ integrity, which are known to limit protrusive activity mediated by Rac (Harris and Tepass, 2010). Taken together, these findings indicate that Cyst is required for the normal association of actomyosin with apical AJs and support a model positing that
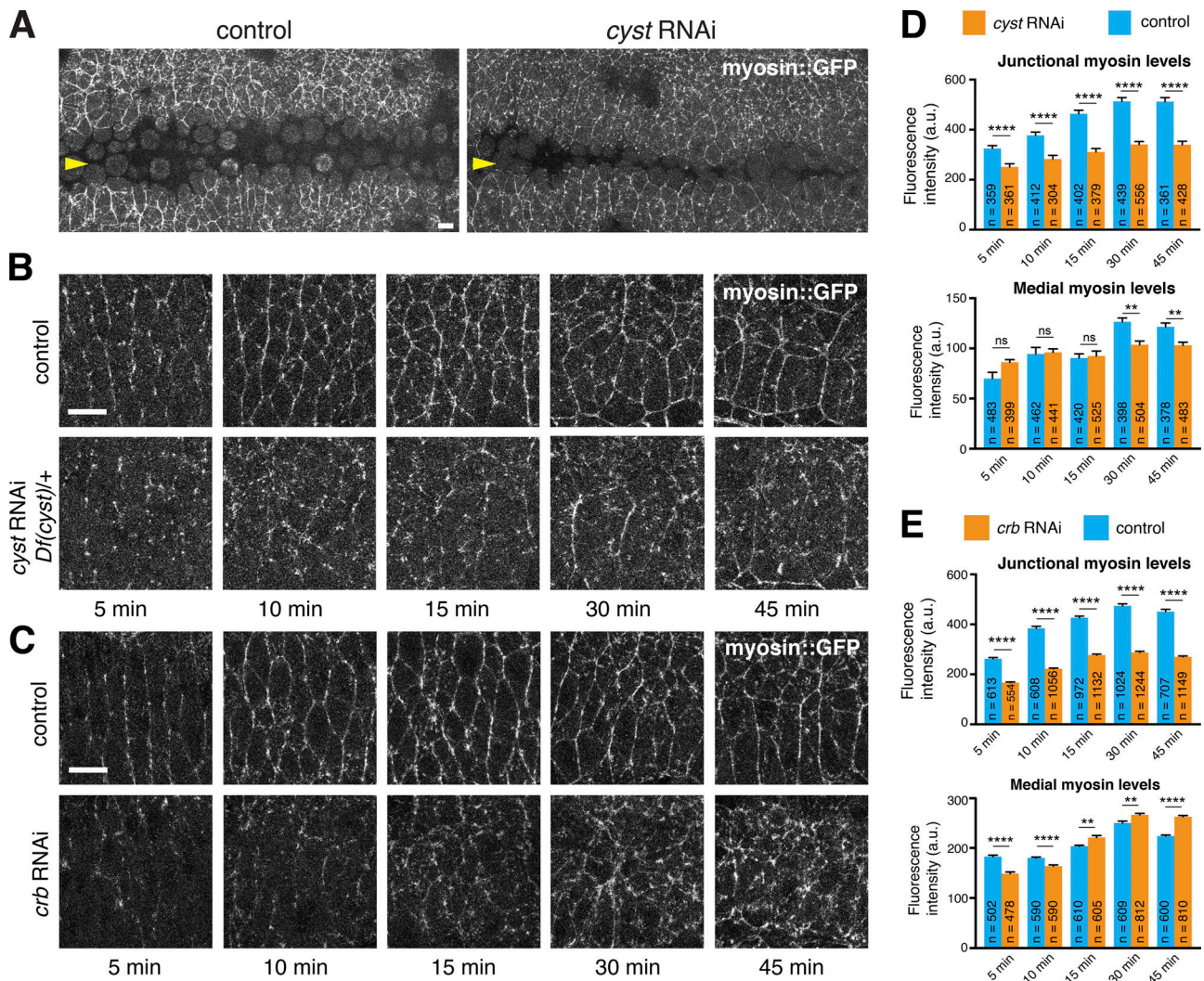
Figure 9. **Cyst regulates actomyosin dynamics at AJs. (A)** Z-projections taken from live stage-8 embryos expressing myosin::GFP (Sqh::GFP) in a control (n = 3) or *cyst* RNAi (n = 3) background. The ventral ectoderm is shown with the arrowhead pointing to the ventral midline. The *cyst* RNAi embryo shows a reduction of myosin::GFP. Scale bar, 10 µm. **(B)** Stills of time-lapse videos (Videos 5 and 6) showing myosin::GFP in a control embryo (maternal expression of mCherry RNAi) and in a *cyst*-depleted embryo (maternal expression of *cyst* RNAi in a *Df(cysts)/+* mother). Time is minutes after the onset of germband extension. In the control, multicellular myosin II cables form at the anterior-posterior cell–cell contacts during axis elongation. Junctional myosin levels and multicellular cables are reduced in *cyst*-depleted embryos. Scale bar, 10 µm. **(C)** Stills of time-lapse videos (Videos 7 and 8) showing myosin::GFP expression in a control embryo (H_2O injected) and in a *crb* dsRNA–injected embryo. Time is minutes after the onset of germband extension. Junctional myosin levels are reduced, and medial myosin levels gradually become enhanced in the *crb*-depleted embryo. **(D)** Quantification of junctional and medial myosin levels in control and *cyst*-depleted embryos at the time points indicated in B. Bars indicate mean ± SEM. Three embryos per condition; n values indicate number of cell edges analyzed for junctional myosin and number of apical surface areas analyzed for medial myosin. For junctional myosin, from left to right: ****, $P = 4.2 \times 10^{-4}$, 5.9×10^{-5}, 3.10^{-16}, 4.2×10^{-21}, and 3.4×10^{-16} (Kolmogorov–Smirnov test); for medial myosin, from left to right: ns, $P = 0.19$, $P = 0.59$, and $P = 0.99$; **, $P = 6 \times 10^{-2}$ (Kolmogorov–Smirnov test). **(E)** Quantification of junctional and medial myosin levels in control and *crb* RNAi embryos at the time points indicated in C. Bars indicate mean ± SEM. Three to five embryos per condition; n values indicate number of cell edges analyzed for junctional myosin and number of apical surface areas analyzed for medial myosin. For junctional myosin, from left to right: ****, $P = 6.5 \times 10^{-53}$, 5.5×10^{-72}, 2.5×10^{-60}, 7.2×10^{-66}, and 3.0×10^{-62} (Kolmogorov–Smirnov test); for medial myosin, from left to right: ****, $P = 1.10^{-6}$ and 8.8×10^{-8}; **, 2×10^{-3} and 10^{-3}; ****, $P = 2.7 \times 10^{-9}$ (Kolmogorov–Smirnov test).

Cyst couples the apical Crb complex to junctional Rho1 activity and AJ stability.

Discussion

Cyst links epithelial polarity, AJ stability, and actomyosin remodeling

Antagonistic interactions between apical and basolateral polarity regulators position AJs at the apico-lateral membrane to form a junctional complex. In turn, AJs are thought to maintain apical-basal polarity through the segregation of the apical and basolateral membrane domains, organization of the cytoskeleton, and direct polarity by acting as signaling centers for polarity complexes (Harris and Tepass, 2010; Laprise and Tepass, 2011; Harris, 2012; Tepass, 2012). Although a number of *Drosophila* RhoGEFs and RhoGAPs have been implicated in epithelial polarity and AJ stability (McCormack et al., 2013; Mack and Georgiou, 2014), no single RhoGEF or RhoGAP has been found
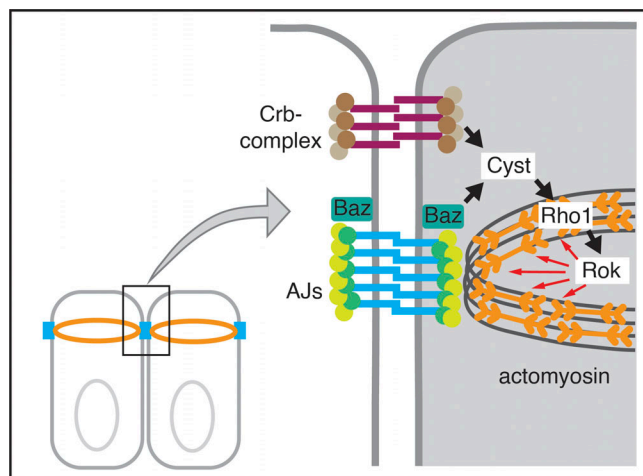
Figure 10. **Model of Cyst function in the *Drosophila* embryo.** The Crb complex and Baz recruit the RhoGEF Cyst to the apicolateral membrane where it activates Rho1 and myosin II, supporting junctional and epithelial integrity.

to phenocopy the polarity or junctional defects that are seen in embryos compromised for factors such as Crb, aPKC, or E-cadherin (Tepaß and Knust, 1990; Tepass et al., 1996; Uemura et al., 1996; Hutterer et al., 2004). Our findings suggest that loss of the RhoGEF Cyst causes a polarity phenotype strikingly similar to the loss of core apical polarity proteins. Moreover, we find that Cyst is recruited to the apico-lateral cortex by the action of polarity proteins and, by activating Rho1, stabilizes AJ-associated actomyosin, which supports junctional and epithelial integrity.

In Cyst-compromised embryos, AJ formation is disrupted in early gastrulation, and AJs do not form a circumferential belt. These defects in AJ assembly or stability correlate with reduced and irregular myosin accumulation at the apico-lateral cortex. Given the molecular function of Cyst as a GEF for Rho1, loss of myosin activity is presumably the immediate cause for the defects in AJ formation and the subsequent loss of apicobasal polarity in many epithelial cells. *crb*-depleted embryos failed to recruit Cyst to apical junctions and showed a similar decline in junctional myosin. Therefore, a major function of the apical Crb polarity complex appears to be the Cyst-mediated support of junctional actomyosin (Fig. 10).

While many cells in *crb* or *cyst* mutants undergo programmed cell death, others retain or recover polarity and form small epithelial cysts, a process seen from mid-embryogenesis (post-gastrulation stages) onward. Several polarity proteins such as Crb, Sdt, and Baz are needed for normal epithelial polarization in early embryos but are not essential for polarization in post-gastrulation embryos, which explains the ability of some epithelial cells in these mutants to form epithelial cysts with normal polarization (Bilder et al., 2003; Tanentzapf and Tepass, 2003; Laprise et al., 2009). In fact, when programmed cell death is suppressed, cyst formation is shown by all epithelial cells in *crb* mutants (Tanentzapf and Tepass, 2003). Formation of epithelial cysts seen in *cyst* mutant embryos therefore suggests that Cyst is also not essential for epithelial polarity in late embryos. This

view is supported by the decline of Cyst protein accumulation at AJs seen in late embryos.

Several observations, including the genetic interaction of *cyst* with genes encoding basolateral polarity proteins, the dependence of the junctional localization of Cyst on the apical polarity proteins Baz and Crb, the physical interactions between Cyst and apical polarity proteins, and the function of Cyst in stabilizing AJs, indicate that Cyst is an integral part of the apical polarity machinery in early *Drosophila* embryos. A particularly striking finding was the complete suppression of the *cyst* phenotype by codepletion of the basolateral polarity proteins Scrib or Lgl, seen in double-mutant embryos that showed phenotypes indistinguishable from single *scrib* or *lgl* mutants. This mimics previous observations with double mutants of *crb* or *sdt* and *scrib*, *lgl* or *discs large* (Bilder et al., 2003; Tanentzapf and Tepass, 2003). Moreover, we found that a reduction of aPKC enhanced Baz mislocalization in Cyst-compromised embryos, suggesting that aPKC cooperates with Cyst and acts upstream or in parallel to Cyst to organize Baz. These findings emphasize that Cyst, similar to Crb and aPKC, is a component of a negative feedback circuit between apical and basolateral regulatory networks that govern epithelial polarity. The dependence of Cyst localization on Crb and Baz suggests that Cyst acts downstream of these two proteins. Once polarized, Cyst appears to maintain polarity and junctional stability through actomyosin remodeling.

A multifaceted mechanism of Cyst junctional recruitment

Our in vivo structure–function data indicate that the C-terminal region is essential for Cyst activity. Moreover, we found that the C-terminal region of Cyst can oligomerize, potentially facilitated by the CC domain (Schultz et al., 1998; Letunic et al., 2015). We speculate that clustering of Cyst could enhance its cortical association. The Crb complex protein Patj represents one possible anchor for Cyst clusters at the cortex. Our biochemical data show that the Cyst C-terminal region is sufficient for interactions with Patj. Patj has been implicated as a myosin II activator in the embryo (Sen et al., 2012). We propose therefore that Crb, Patj, and Cyst form a complex that organizes junctional actomyosin. However, as Patj is not essential for embryonic survival (Sen et al., 2012), Cyst may interact with additional binding partners within the Crb complex. Another apical binding partner for Cyst is Baz/Par3, which is required for Cyst cortical recruitment, coprecipitates with the Cyst C-terminal region, and coaggregates with Cyst in HeLa cells.

A recent independent study also arrived at the conclusion that Cyst activates Rho1 at AJs during germband extension in the *Drosophila* embryo (de Las Bayonas et al., 2019). It is further shown that depletion of Cyst acts downstream of a G protein–coupled receptor (GPCR) and the Gβ13F/Gγ1 heterotrimeric G protein in directing cell rearrangements promoting germband extension, and that germband extension is somewhat reduced when Cyst is depleted. Loss of Gγ1 causes an ~20% reduction in Cyst junctional enrichment (de Las Bayonas et al., 2019). These and our data suggest that the normal junctional recruitment of Cyst requires at least three distinct inputs: interactions with Baz/Par3 and the Crb complex, and heterotrimeric G protein signaling.

Silver et al.
RhoGEF Cysts links polarity to junctional myosin

Journal of Cell Biology
https://doi.org/10.1083/jcb.201807106
3408

The GEF activity of Cyst targets Rho1

We found that Cyst becomes enriched at the apico-lateral cortex after the mesoderm and endoderm have invaginated and the germband starts to elongate. This localization coincides with the assembly of the apical-cortical actomyosin network. Rho–Rho kinase signaling plays a critical role in the activation of myosin II in this process (Lecuit and Lenne, 2007; Amano et al., 2010; Harris and Tepass, 2010; Lecuit and Yap, 2015). Our structure–function analysis showed that Cyst contains an essential RhoGEF domain as predicted, and the use of Rho activity probes, genetic interactions, and biochemical assays showed that Cyst preferentially targets Rho1. Although our biochemical assay also revealed stimulation of Rac1 activity by Cyst, all other data point to Rho1 as the primary target of Cyst. We propose therefore that Cyst activates Rho1 to organize actomyosin at the cortex at a time when AJs assemble into a circumferential belt (stages 6/7). Consistent with this, we found that Cyst is important for maintaining normal cortical levels of myosin II. A similar loss in junctional myosin was also observed in Crb-compromised embryos in line with our finding that Crb is required for Cyst junctional recruitment. The *cyst* mutant phenotype suggests that Cyst is the key RhoGEF that activates Rho1 at ectodermal AJs. In contrast, RhoGEF2 functions in the mesoderm and ectoderm, where it becomes apico-cortically enriched and activates Rho1 to recruit myosin II to the apical-medial cortex (Padash Barmchi et al., 2005; Manning and Rogers, 2014; Kerridge et al., 2016; de Las Bayonas et al., 2019). Thus, RhoGEF and Cyst act in parallel on Rho1 to orchestrate the balance of cortical and medial actomyosin dynamics.

Cyst and its mammalian orthologue p114RhoGEF share a conserved function

Cyst is the single orthologue of a group of four mammalian RhoGEFs that target RhoA in cell culture (Cook et al., 2014). One of the mammalian orthologues (p114RhoGEF) stabilizes tight junctions and AJs through organization of the actin cytoskeleton associated with cellular junctions (Nakajima and Tanoue, 2010, 2011; Terry et al., 2011; Acharya et al., 2018). p114RhoGEF is recruited to apical junctions through a mechanism involving CRB3A, Ehm2/Lulu2, Par3, Patj (Nakajima and Tanoue, 2011; Loie et al., 2015), the heterotrimeric G protein Gα12, and the GPCR Sphingosine-1 phosphate receptor 2 (Acharya et al., 2018). p114RhoGEF requires the polarity regulator Ehm2/Lulu2 (a homologue of *Drosophila* Yrt) to activate RhoA (Nakajima and Tanoue, 2010, 2011). In contrast, we did not detect genetic or biochemical interactions between Cyst and Yrt in *Drosophila*. Recently, *ARHGEF18*, the human orthologue of *p114RhoGEF*, was identified as a gene associated with retinal degeneration (Arno et al., 2017), and a fish orthologue is required to maintain epithelial integrity of the retina (Herder et al., 2013). *ARHGEF18* mutant retinal defects closely resemble those found in patients carrying mutations in the *crb* homologue *CRB1* (Arno et al., 2017). We conclude that the function of Cyst and p114RhoGEF/ARHGEF18 in coupling apical polarity proteins and GPCR signaling to junctional Rho activity and actomyosin function is conserved between flies and vertebrates and likely contributes to retinal

health in humans, although some of the molecular interactions may have shifted in relative importance.

The other mammalian orthologues of Cyst, p190RhoGEF, AKAP-13, and GEF-H1 have not been implicated as regulators of epithelial polarity (Cook et al., 2014). GEF-H1 (also known as ARHGEF2 and Lfc) was shown to be inactive at mature tight junctions (Aijaz et al., 2005; Terry et al., 2011). In this case, the tight junction protein Cingulin forms a complex with GEF-H1, preventing it from activating RhoA (Aijaz et al., 2005; Terry et al., 2011). Instead, GEF-H1 is thought to promote junction disassembly and cell proliferation, presumably through an association with the mitotic spindle (Ren et al., 1998; Aijaz et al., 2005; Samarin et al., 2007; Birkenfeld et al., 2008; Terry et al., 2011; Cullis et al., 2014). GEF-H1 was also implicated in the morphogenesis of the vertebrate neural tube (Itoh et al., 2014), and in the regulation of RhoA activity during cytokinesis (Birkenfeld et al., 2007). Like GEF-H1, p190RhoGEF has been shown to associate with microtubules (Birkenfeld et al., 2008). GEF-H1 and AKAP-13 were also found to serve additional functions independent of their RhoGEF activity (Shibolet et al., 2007; Cullis et al., 2014). Whether and how Cyst might consolidate the functions of its various mammalian orthologues remains to be explored.

Materials and methods

Drosophila genetics

Flies were raised on standard media at 25°C. Cyst was depleted in the germline of females carrying mat-GAL4 (*P{matα4-GAL-VP16}67*; *P{matα4-GAL-VP16}15*; Häcker and Perrimon, 1998) and *cyst* RNAi (Valium20-SH00146.N-40 inserted at attP40 on the second chromosome; Ni et al., 2011; Transgenic RNAi Project [TRiP]). Virgin females were crossed to males carrying *cyst* RNAi to produce *cyst* RNAi embryos. A second insertion of the same *cyst* shRNA (Valium22-SH00146.N2) gave similar results.

The following fly lines were used: *cyst¹* FRT40A/CyO (this work); *cyst* RNAi (Valium20-SH00146.N-40, Bloomington Drosophila Stock Center [BDSC] #38292); *Df(cyst)* (*Df(2L)BSC301*, BDSC #23684); *Df(cyst)* (*Df(2L)BSC301*) *cyst* RNAi (Valium22-SH00146.N2, BDSC #41578); *scrib* RNAi (Valium20-SH02077.N BDSC #35748); *y w; lgl⁴* FRT40A (gift from T. Xu, Yale University, New Haven, CT); *y w; lgl⁴ cyst¹* FRT40A; *aPKC^{K06403}* (gift of C. Doe, University of Oregon, Eugene, OR), *mCherry* shRNA (BDSC #35785); UAS-PKNG58A::Venus (Simões et al., 2014); UAS-Anillin-RBD::GFP (Munjal et al., 2015); and *histone::GFP* (gift of A. Wilde, University of Toronto, Toronto, ON, Canada).

shg>DEcad::GFP (DEcad::GFP controlled by its endogenous promoter; Huang et al., 2009) and *sqh>sqh::GFP* (Sph controlled by its endogenous promoter; Royou et al., 1999) were recombined with the mat-GAL4 driver. *Utrophin::GFP cyst* RNAi males were crossed to the mat-GAL4 driver, and then crossed to *cyst* RNAi males to generate *cyst* RNAi embryos expressing *Utrophin::GFP* (eGFP fused to the actin binding domain of human Utrophin; Rauzi et al., 2010). Cyst overexpression UAS constructs were driven by *da-GAL4* (Wodarz et al., 1995) or mat-GAL4. To examine genetic interactions between *cyst* and Rho GTPases, we crossed females expressing UAS-controlled Cyst or

Cyst-N with the mat-GAL4 driver to P{UAS-Rho1.N19}1.3 (Strutt et al., 1997), P{UAS-Rac1.L89.}6, or P{UAS-Cdc42.N17} (Luo et al., 1994) males.

Generation of the *cyst[1]* mutation and mutant germline clones
We generated a null mutation for *cyst* (*cyst[1]*) using the RNA-guided CRISPR/Cas9 system (Gratz et al., 2013; GenetiVision Corp.). The second exon of *cyst* was targeted using gRNA1 (5′-GTTAGCAATAACTAATCGCA-3′) and gRNA2 (5′-AGCTCCTCG AGCCAAGCCCG-3′) and replaced with a 3xP3-GFP cassette. Sequencing confirmed the following breakpoints: 19503155 and 19506410. To generate germline clones for *cyst[1]* or *lgl[4] cyst[1]* mutations, we crossed *w; cyst[1] FRT40A/CyO* or *w; lgl[4] cyst[1] FRT40A/ CyO* to Ovo[D] males (*y[1] w[*] P{ry[+t7.2]=hsFLP}12; 2121P{w[+mC] =ovoD1-18}2La P{w[+mC]=ovoD1-18}2Lb P{ry[+t7.2]=neoFRT}40A*). Ovo[D] males resulted from a cross of BDSC stocks #1929 and #2121. FLP/FRT-mediated mitotic recombination in resulting females was induced by two heat shocks in a 37°C water bath for 1 h at late second and late third larval instar (Chou and Perrimon, 1992). Females were outcrossed to heterozygous *cyst[1]* or *lgl[4] cyst[1]* mutant males, respectively, and eggs were collected for analysis.

Preparation of cuticle
To prepare the cuticle of fully differentiated embryos (Wieschaus and Nüsslein-Volhard, 1986), embryos were aged for 36–48 h after egg collection at 25°C, washed, and dechorionated in a 2% bleach solution for 5 min. After washing with double-distilled H_2O, eggs were transferred onto a slide into a 1:1 mixture of Hoyer's medium and lactic acid, covered with a coverslip, and incubated overnight at 85°C. Images were taken with a Carl Zeiss Axiophot2 microscope using a phase-contrast 20× lens (NA 0.5). Pictures were recorded with a Canon Rebel XSi camera using Canon software and processed in Adobe Photoshop and Illustrator.

Molecular biology
Genomic rescue constructs
An ~7.0-kb fragment (genomic region 19509164–19502181) encompassing the *cyst* gene was amplified from BACR27M12 (BACPAC) and recombined into pENTR221 (Invitrogen). To confer RNAi resistance on the resulting Entry Clone, silent mutations were introduced at two distinct sites corresponding to SH00146.N (TRiP). All other genomic constructs were derived from this Entry Clone. The GFP-tagged full-length construct was generated by inserting *Drosophila* codon-optimized superfolder GFP (Pédelacq et al., 2006) in between the ATG and the second codon of *cyst*. The GFP-tagged deletion constructs were generated by replacing the domains described in Fig. 6 A with superfolder GFP. In all constructs, an S(GGGGS)$_2$ linker was introduced in between GFP and Cyst, and in CystΔN, the intron was left intact to preserve potential regulatory sequences. Finally, all Entry Clones were recombined into the *Drosophila* transformation vector pBID-G (Wang et al., 2012b).

UAS constructs
The *cyst* ORF including the intron was amplified from the first Entry Clone described above containing Cyst[R] and recombined

into pDONR221. The intron was then deleted from this Entry Clone to give the full-length *cyst[R]* ORF. A fragment corresponding to Cyst[R]-N was amplified from this Entry Clone and recombined into pDONR221. The resulting Entry Clones for Cyst[R] and Cyst[R]-N were recombined into a destination vector containing the UASp promoter (Rørth, 1998) and an N-terminal 3×HA tag separated from Cyst[R] by an SGGGS linker (unpublished data). Cloning was performed using Gateway (Invitrogen) or In-Fusion (Clontech) cloning kits. All plasmids generated by PCR were sequence-verified along the entire length of the insert. Plasmid and primer sequences are available on request. Transgenes were placed in attP40 by ΦC31-mediated transgenesis.

Other mammalian expression constructs
To generate the expression constructs used for experiments shown in Fig. 8 (C–E) and Fig. S2, we cloned full-length cDNAs encoding *Drosophila* Rho1, Rac1, Cdc42, and Cyst by RT-PCR using a sequenced strains (BDSC #2057), and then subcloned into the pCR-BluntII-TOPO vector (Invitrogen). All PCR fragments were validated by DNA sequencing. Full-length and deletion constructs were subcloned into a pEGFP vector (Clontech) for N-terminal EGFP fusion protein and a modified pCAGGS vector that contained an N-terminal 3xFLAG tag. For immunoprecipitation experiments (Fig. 7, B–D), Cyst[R] constructs were subcloned into pcDNA3-3xFLAG and pcDNA3-GFP vectors. pEGFP and pcDNA3 expression vectors are driven by the cytomegalovirus promoter, and pCAGGS expression vector is driven by a hybrid promoter consisting of cytomegalovirus early enhancer and chicken β-actin (CAG promoter). pEGFP-LARF-DH-PH and pEGFP-INTS2-DH-PH were generously provided by K. Kaibuchi (Nagoya University, Nagoya, Japan), pEGFP-STEF-ΔN by M. Hoshino (National Institute of Neuroscience, Tokyo, Japan), and pEGFP-Par3 by S. Ohno (Yokohama City University, Yokohama, Japan).

Injection of dsRNA has been previously described for *baz* (Simões et al., 2010). The dsRNA against *crb* was in vitro transcribed from a template that was PCR amplified from genomic DNA using the following *crb* primers fused to a T7 promoter sequence at the 5′ end: forward 5′-CGAGCCATGTCGGAATGG ATCAACC-3′; reverse 5′-GTCGCTCTTCCGGCGGTGGCTTCAG-3′.

Cell culture and immunoprecipitation LC-MS/MS
HEK293T and HeLa cells were cultured in DMEM (Fujifilm Wako Chemicals) with 10% FBS (Thermo Fisher Scientific), penicillin, and streptomycin, and transfection was performed using polyethyleneimine (Polysciences Warrington). Cells were transfected in 10-cm Petri dishes and incubated with serum-free DMEM for 4 h before processing.

For the LC-MS/MS assay, HEK293T cells were cotransfected with FLAG-tagged versions of *Drosophila* Rho1, Rac1, or Cdc42 and either the GFP-tagged Cyst fragments shown in Fig. 8 C or GFP-tagged versions of the mammalian GEFs LARG-DH-PH, STEF-ΔN, or INTS2-DH-PH, or GFP alone. For coimmunoprecipitation experiments (Fig. 7, B–D), cells were cotransfected with GFP-tagged Cyst fragments and FLAG::Cyst-C (as described above) or FLAG-tagged *Drosophila* Baz or Patj. Cells were rinsed once with ice-cold PBS and extracted with ice-cold lysis buffer B (10 mM Tris/HCl, pH 7.5, 300 mM NaCl, 10 mM $MgCl_2$, 1%

Triton X-100, 50 µg/ml PMSF, and Complete Protease Inhibitor Cocktail [Roche]) and cleared by centrifugation at 15,000 rpm for 10 min at 4°C. For immunoprecipitation, primary antibodies were added to lysates and incubated with rotation for 2 h at 4°C.

For the LC-MS/MS assay, cell lysates were incubated with FLAG M2 Agarose (Sigma-Aldrich, Canada) to precipitate the FLAG-tagged GTPases for 2 h at 4°C. The beads were washed three times with lysis buffer B and further washed two times with buffer C (10 mM ammonium bicarbonate and 5 mM MgCl$_2$). The bound nucleotides were eluted with 80 µl methanol and 80 µl chloroform followed by shaking for 30 min at room temperature. 80 µl of water was added, and the supernatants were collected after centrifugation at 10,000 rpm for 10 min, followed by vacuum centrifuge drying. The pellets were resuspended in 15 µl of 20 mM ammonium bicarbonate, and guanine nucleotides were quantified by LC-MS/MS.

The chromatographic separation was performed on an Acquity HSS T3 column (100 × 2.1 mm, 1.8-µm particles [Waters]) at 30°C under isocratic conditions (0.3 ml/min, 10 mM ammonium bicarbonate) using an Acquity UPLC H-Class System (Waters). MS analysis was performed using a Xevo TQD triple-quadrupole mass spectrometer (Waters) coupled with an electrospray ionization source in the positive ion mode. The MRM transitions of m/z 524→152.1 and m/z 444.1→152.1 were used to quantify GTP and GDP, respectively. Sample concentrations were calculated from the standard curve obtained from serial dilution of each nucleotide standard (Sigma-Aldrich, Canada). Analytical conditions were optimized using standard solutions. The percentage of GTP-bound small GTPases was expressed as GTP/(GTP + GDP) × 100, which normalizes for the amount of immunoprecipitated GTPase protein in each sample. Values were further normalized to that of the Cyst N-terminal fragment or GFP controls. Error bars represent the SD of four independent experiments.

Antibody staining
Drosophila embryos were heat-fixed (Tepass, 1996) or fixed for 20 min in 3.7% formaldehyde diluted in a 1:1 PBS:heptane mixture. To visualize the PKNG58A::Venus sensor, embryos were fixed in a 1:1 mixture of 3.7% formaldehyde and phosphate buffer, pH 7.4, and heptane for 40 min under agitation followed by hand devitellization. Primary antibodies used were anti-Crb (rat polyclonal, extracellular F3; 1:1,000; Pellikka et al., 2002), anti-Yrt (guinea pig polyclonal, GP7; 1:500; Laprise et al., 2006), anti-Arm (mouse monoclonal, N2-7A1; 1:50; Developmental Studies Hybridoma Bank), anti-HA (rat monoclonal, 3F10; 1:500; Roche), anti-Baz (1:3,500), anti-Baz (GP, 1:500, a gift from Jennifer Zallen, Memorial Sloan Kettering Cancer Center, New York, NY), anti-PKCζ (C-20; 1:100; rabbit polyclonal; Santa Cruz), and anti-Dlg (1:100; mouse; Developmental Studies Hybridoma Bank).

Transfected HeLa cells were fixed with 3.7% formaldehyde in PBS for 10 min at room temperature, followed by treatment with 0.2% Triton X-100 in PBS with 2 mg/ml BSA for 10 min, and processed for immunostaining. Primary and secondary antibodies used were chicken anti-GFP (Abcam), mouse anti-FLAG M2 (Sigma-Aldrich,), Alexa Fluor 488 goat anti-chicken IgY, and Alexa Fluor 555 goat anti-mouse IgG (Thermo Fisher Scientific). F-actin was visualized with Alexa Fluor 555

phalloidin (Thermo Fisher Scientific). Samples were mounted in 50% glycerol in PBS.

Imaging and signal intensity quantification
Except for Fig. 4, imaging of live or fixed samples was done with a Leica TCS SP8 scanning confocal microscopy with 40×, 63×, and 100× objectives (HC PL APO CS2 with NAs of 1.30, 1.40, and 1.40 respectively). Time-lapse acquisitions were done in a manner similar to that previously described (Blankenship et al., 2006). Three to five live embryos were examined for each genotype. A 0.5-µm step was used to collect z-stacks. Stills and videos were assembled from maximum-intensity projections of six apical planes (ImageJ; National Institutes of Health). Supplemental videos shown were downsampled in iMovie (Apple). Original videos are available upon request. Adobe Photoshop and Adobe Illustrator were used to process and arrange images. The same settings were applied to all images within an experimental series. The average fluorescence intensity of junctional and medial Sqh::GFP, junctional Anillin-RBD::GFP, and PKNG58A::Venus was quantified in segmented cells using Matlab and the script SIESTA (scientific image segmentation and analysis; Fernandez-Gonzalez and Zallen, 2011). To quantify junctional Sqh::GFP, Anillin-RBD::GFP, and PKNG58A::Venus, we manually drew 3-pixel-wide lines (180 nm/pixel) for cell edges at the indicated time points to obtain the mean pixel intensity for a cell edge. The mode (cytoplasmic) intensity was subtracted for background correction. To quantify medial Sqh::GFP mean protein levels, each cell was divided into two compartments (Fernandez-Gonzalez and Zallen, 2011). The junctional compartment was determined by a 3-pixel-wide (0.54 µm) dilation of the cell outline identified using watershed or LiveWire segmentation in SIESTA. The medial compartment was obtained by inverting a binary image representing the junctional compartment. Given the dynamic nature of medial Sqh::GFP, we quantified it as the mean pixel intensity in the medial compartment in 10 consecutive time frames per cell (total elapsed time of 5 min per data point), centered at the indicated time points, and subtracted the mode (cytoplasmic) intensity for background correction.

For data presented in Fig. 4, we used a spinning disk confocal microscope (Quorum Technologies) with a 63× Plan Apochromat objective (NA 1.4; Carl Zeiss), piezo top plate, and electron multiplier charge-coupled device camera (Hamamatsu Photonics). Baz puncta were quantified by dividing the number of cells with two Baz puncta by the total number of cells. aPKC levels were the average difference between the cell cortical and cytoplasmic signals of five different cells per embryo, normalized to internal GFP-expressing controls. Cytochalasin D and DMSO were diluted 2,000 times in an NaCl-octane solution before embryo incubations. To quantify apical aPKC levels, the apicolateral section with the strongest aPKC signal was selected for each embryo. Within each embryo section, regions of interest were selected for the cell cortex and for the neighboring cytoplasm of five different cells. The cytoplasmic values were subtracted from the cortical values for background correction, and the five corrected values were averaged to produce one quantification of apical aPKC level per embryo. These quantifications were

normalized to the average of the quantifications for control embryos. Controls were costained and comounted for Fig. 4 D and were treated, stained, and mounted in parallel preparations for Fig. 4 F.

Data shown in Fig. S2 were acquired with a LSM700 laser scanning confocal microscope (Carl Zeiss) with a 40× C-Apochromat water-immersion objective (NA 1.2). Images were obtained using ZEN2009 software (Carl Zeiss) and processed with Adobe Photoshop.

Statistics
Statistical analysis was performed in Microsoft Excel or Prism v7 (GraphPad). We used Student's t test for pairwise comparisons in Figs. 4 and 8 D, with data presented as mean + SD. We used the nonparametric Kolmogorov–Smirnov test for Figs. 8 B, 9 (D and E), and S3 B, with data presented as mean + SEM.

Online supplemental material
Figure S1 shows aPKC distribution in *cyst* RNAi embryos. Figure S2 shows Cyst coaggregates with Par3 and elicits formation of ruffles and stress fibers. Figure S3 shows interactions between Cyst and Rho1. Figure S4 shows that Cyst regulates actin dynamics. Video 1 shows DEcad::GFP in control embryo. Video 2 shows DEcad::GFP in *cyst* RNAi embryo. Video 3 shows AnillinRBD::GFP biosensor expression in a control embryo. Video 4 shows AnillinRBD::GFP biosensor expression in a *cyst* RNAi embryo. Video 5 shows myosin II dynamics in a mock-RNAi control embryo. Video 6 shows myosin II dynamics in a *cyst* RNAi embryo. Video 7 shows myosin II dynamics in a control embryo. Video 8 shows myosin II dynamics in a *crb* RNAi embryo. Video 9 shows actin dynamics in control embryo. Video 10 shows actin dynamics in a *cyst* RNAi embryo.

References
Acharya, B.R., A. Nestor-Bergmann, X. Liang, S. Gupta, K. Duszyc, E. Gauquelin, G.A. Gomez, S. Budnar, P. Marcq, O.E. Jensen, et al. 2018. A mechanosensitive RhoA pathway that protects epithelia against acute tensile stress. *Dev. Cell.* 47:439–452.e6. https://doi.org/10.1016/j.devcel.2018.09.016

Aijaz, S., F. D'Atri, S. Citi, M.S. Balda, and K. Matter. 2005. Binding of GEF-H1 to the tight junction-associated adaptor cingulin results in inhibition of Rho signaling and G1/S phase transition. *Dev. Cell.* 8:777–786. https://doi.org/10.1016/j.devcel.2005.03.003

Amano, M., M. Nakayama, and K. Kaibuchi. 2010. Rho-kinase/ROCK: A key regulator of the cytoskeleton and cell polarity. *Cytoskeleton (Hoboken).* 67:545–554. https://doi.org/10.1002/cm.20472

Arno, G., K.J. Carss, S. Hull, C. Zihni, A.G. Robson, A. Fiorentino, A.J. Hardcastle, G.E. Holder, M.E. Cheetham, V. Plagnol, et al. NIHR Bioresource - Rare Diseases Consortium. 2017. Biallelic mutation of ARHGEF18, involved in the determination of epithelial apicobasal polarity, causes adult-onset retinal degeneration. *Am. J. Hum. Genet.* 100:334–342. https://doi.org/10.1016/j.ajhg.2016.12.014

Aspenström, P. 1999. Effectors for the rho GTPases. *Curr. Opin. Cell Biol.* 11:95–102. https://doi.org/10.1016/S0955-0674(99)80011-8

Benton, R., and D. St Johnston. 2003. Drosophila PAR-1 and 14-3-3 inhibit Bazooka/PAR-3 to establish complementary cortical domains in polarized cells. *Cell.* 115:691–704. https://doi.org/10.1016/S0092-8674(03)00938-3

Bilder, D., and N. Perrimon. 2000. Localization of apical epithelial determinants by the basolateral PDZ protein Scribble. *Nature.* 403:676–680. https://doi.org/10.1038/35001108

Bilder, D., M. Schober, and N. Perrimon. 2003. Integrated activity of PDZ protein complexes regulates epithelial polarity. *Nat. Cell Biol.* 5:53–58. https://doi.org/10.1038/ncb897

Birkenfeld, J., P. Nalbant, B.P. Bohl, O. Pertz, K.M. Hahn, and G.M. Bokoch. 2007. GEF-H1 modulates localized RhoA activation during cytokinesis under the control of mitotic kinases. *Dev. Cell.* 12:699–712. https://doi.org/10.1016/j.devcel.2007.03.014

Birkenfeld, J., P. Nalbant, S.H. Yoon, and G.M. Bokoch. 2008. Cellular functions of GEF-H1, a microtubule-regulated Rho-GEF: is altered GEF-H1 activity a crucial determinant of disease pathogenesis? *Trends Cell Biol.* 18:210–219. https://doi.org/10.1016/j.tcb.2008.02.006

Blankenship, J.T., S.T. Backovic, J.S. Sanny, O. Weitz, and J.A. Zallen. 2006. Multicellular rosette formation links planar cell polarity to tissue morphogenesis. *Dev. Cell.* 11:459–470. https://doi.org/10.1016/j.devcel.2006.09.007

Chartier, F.J.M., É.J.L. Hardy, and P. Laprise. 2011. Crumbs controls epithelial integrity by inhibiting Rac1 and PI3K. *J. Cell Sci.* 124:3393–3398. https://doi.org/10.1242/jcs.092601

Chou, T.B., and N. Perrimon. 1992. Use of a yeast site-specific recombinase to produce female germline chimeras in Drosophila. *Genetics.* 131:643–653.

Cook, D.R., K.L. Rossman, and C.J. Der. 2014. Rho guanine nucleotide exchange factors: regulators of Rho GTPase activity in development and disease. *Oncogene.* 33:4021–4035. https://doi.org/10.1038/onc.2013.362

Cox, R.T., C. Kirkpatrick, and M. Peifer. 1996. Armadillo is required for adherens junction assembly, cell polarity, and morphogenesis during Drosophila embryogenesis. *J. Cell Biol.* 134:133–148. https://doi.org/10.1083/jcb.134.1.133

Cullis, J., D. Meiri, M.J. Sandi, N. Radulovich, O.A. Kent, M. Medrano, D. Mokady, J. Normand, J. Larose, R. Marcotte, et al. 2014. The RhoGEF GEF-H1 is required for oncogenic RAS signaling via KSR-1. *Cancer Cell.* 25:181–195. https://doi.org/10.1016/j.ccr.2014.01.025

de Las Bayonas, A.G., J.-P. Philippe, A.C. Lellouch, and T. Lecuit. 2019. Distinct RhoGEFs activate apical and junctional actomyosin contractility under control of G proteins during epithelial morphogenesis. *bioRxiv.* 566919. Preprint March 4, 2019.

Fernandez-Gonzalez, R., and J.A. Zallen. 2011. Oscillatory behaviors and hierarchical assembly of contractile structures in intercalating cells. *Phys. Biol.* 8:045005. https://doi.org/10.1088/1478-3975/8/4/045005

Fletcher, G.C., E.P. Lucas, R. Brain, A. Tournier, and B.J. Thompson. 2012. Positive feedback and mutual antagonism combine to polarize Crumbs in the Drosophila follicle cell epithelium. *Curr. Biol.* 22:1116–1122. https://doi.org/10.1016/j.cub.2012.04.020

Fox, D.T., C.C. Homem, S.H. Myster, F. Wang, E.E. Bain, and M. Peifer. 2005. Rho1 regulates Drosophila adherens junctions independently of p120ctn. *Development.* 132:4819–4831. https://doi.org/10.1242/dev.02056

Gamblin, C.L., E.J. Hardy, F.J. Chartier, N. Bisson, and P. Laprise. 2014. A bidirectional antagonism between aPKC and Yurt regulates epithelial cell polarity. *J. Cell Biol.* 204:487–495. https://doi.org/10.1083/jcb.201308032

Genova, J.L., S. Jong, J.T. Camp, and R.G. Fehon. 2000. Functional analysis of Cdc42 in actin filament assembly, epithelial morphogenesis, and cell signaling during Drosophila development. *Dev. Biol.* 221:181–194. https://doi.org/10.1006/dbio.2000.9671

Gratz, S.J., A.M. Cummings, J.N. Nguyen, D.C. Hamm, L.K. Donohue, M.M. Harrison, J. Wildonger, and K.M. O'Connor-Giles. 2013. Genome engineering of Drosophila with the CRISPR RNA-guided Cas9 nuclease. *Genetics.* 194:1029–1035. https://doi.org/10.1534/genetics.113.152710

Grawe, F., A. Wodarz, B. Lee, E. Knust, and H. Skaer. 1996. The Drosophila genes crumbs and stardust are involved in the biogenesis of adherens junctions. *Development.* 122:951–959.

Greenberg, L., and V. Hatini. 2011. Systematic expression and loss-of-function analysis defines spatially restricted requirements for Drosophila RhoGEFs and RhoGAPs in leg morphogenesis. *Mech. Dev.* 128:5–17. https://doi.org/10.1016/j.mod.2010.09.001

Häcker, U., and N. Perrimon. 1998. DRhoGEF2 encodes a member of the Dbl family of oncogenes and controls cell shape changes during gastrulation in Drosophila. *Genes Dev.* 12:274–284. https://doi.org/10.1101/gad.12.2.274

Hakeda-Suzuki, S., J. Ng, J. Tzu, G. Dietzl, Y. Sun, M. Harms, T. Nardine, L. Luo, and B.J. Dickson. 2002. Rac function and regulation during Drosophila development. *Nature.* 416:438–442. https://doi.org/10.1038/416438a

Hall, A. 2012. Rho family GTPases. *Biochem. Soc. Trans.* 40:1378–1382. https://doi.org/10.1042/BST20120103

Hanna, S., and M. El-Sibai. 2013. Signaling networks of Rho GTPases in cell motility. *Cell. Signal.* 25:1955–1961. https://doi.org/10.1016/j.cellsig.2013.04.009

Harden, N. 2002. Signaling pathways directing the movement and fusion of epithelial sheets: lessons from dorsal closure in Drosophila. *Differentiation.* 70:181–203. https://doi.org/10.1046/j.1432-0436.2002.700408.x

Harris, T., ed. 2012. *Adherens Junctions: From Molecular Mechanisms to Tissue Development and Disease.* Springer Science & Business Media, Berlin. 60 pp.

Harris, K.P., and U. Tepass. 2008. Cdc42 and Par proteins stabilize dynamic adherens junctions in the Drosophila neuroectoderm through regulation of apical endocytosis. *J. Cell Biol.* 183:1129–1143. https://doi.org/10.1083/jcb.200807020

Harris, T.J., and M. Peifer. 2007. aPKC controls microtubule organization to balance adherens junction symmetry and planar polarity during development. *Dev. Cell.* 12:727–738. https://doi.org/10.1016/j.devcel.2007.02.011

Harris, T.J., and U. Tepass. 2010. Adherens junctions: from molecules to morphogenesis. *Nat. Rev. Mol. Cell Biol.* 11:502–514. https://doi.org/10.1038/nrm2927

Herder, C., J.M. Swiercz, C. Müller, R. Peravali, R. Quiring, S. Offermanns, J. Wittbrodt, and F. Loosli. 2013. ArhGEF18 regulates RhoA-Rock2 signaling to maintain neuro-epithelial apico-basal polarity and proliferation. *Development.* 140:2787–2797. https://doi.org/10.1242/dev.096487

Huang, J., W. Zhou, W. Dong, A.M. Watson, and Y. Hong. 2009. From the Cover: Directed, efficient, and versatile modifications of the Drosophila genome by genomic engineering. *Proc. Natl. Acad. Sci. USA.* 106:8284–8289. https://doi.org/10.1073/pnas.0900641106

Hutterer, A., J. Betschinger, M. Petronczki, and J.A. Knoblich. 2004. Sequential roles of Cdc42, Par-6, aPKC, and Lgl in the establishment of epithelial polarity during Drosophila embryogenesis. *Dev. Cell.* 6:845–854. https://doi.org/10.1016/j.devcel.2004.05.003

Itoh, K., O. Ossipova, and S.Y. Sokol. 2014. GEF-H1 functions in apical constriction and cell intercalations and is essential for vertebrate neural tube closure. *J. Cell Sci.* 127:2542–2553. https://doi.org/10.1242/jcs.146811

Jaffe, A.B., and A. Hall. 2005. Rho GTPases: biochemistry and biology. *Annu. Rev. Cell Dev. Biol.* 21:247–269. https://doi.org/10.1146/annurev.cellbio.21.020604.150721

Jiang, T., R.F. McKinley, M.A. McGill, S. Angers, and T.J. Harris. 2015. A Par-1-Par-3-centrosome cell polarity pathway and its tuning for isotropic cell adhesion. *Curr. Biol.* 25:2701–2708. https://doi.org/10.1016/j.cub.2015.08.063

Kerridge, S., A. Munjal, J.M. Philippe, A. Jha, A.G. de las Bayonas, A.J. Saurin, and T. Lecuit. 2016. Modular activation of Rho1 by GPCR signalling imparts polarized myosin II activation during morphogenesis. *Nat. Cell Biol.* 18:261–270. https://doi.org/10.1038/ncb3302

Kolahgar, G., P.L. Bardet, P.F. Langton, C. Alexandre, and J.P. Vincent. 2011. Apical deficiency triggers JNK-dependent apoptosis in the embryonic epidermis of Drosophila. *Development.* 138:3021–3031. https://doi.org/10.1242/dev.059980

Laprise, P., and U. Tepass. 2011. Novel insights into epithelial polarity proteins in Drosophila. *Trends Cell Biol.* 21:401–408. https://doi.org/10.1016/j.tcb.2011.03.005

Laprise, P., S. Beronja, N.F. Silva-Gagliardi, M. Pellikka, A.M. Jensen, C.J. McGlade, and U. Tepass. 2006. The FERM protein Yurt is a negative regulatory component of the Crumbs complex that controls epithelial polarity and apical membrane size. *Dev. Cell.* 11:363–374. https://doi.org/10.1016/j.devcel.2006.06.001

Laprise, P., K.M. Lau, K.P. Harris, N.F. Silva-Gagliardi, S.M. Paul, S. Beronja, G.J. Beitel, C.J. McGlade, and U. Tepass. 2009. Yurt, Coracle, Neurexin IV and the Na(+),K(+)-ATPase form a novel group of epithelial polarity proteins. *Nature.* 459:1141–1145. https://doi.org/10.1038/nature08067

Lecuit, T., and P.F. Lenne. 2007. Cell surface mechanics and the control of cell shape, tissue patterns and morphogenesis. *Nat. Rev. Mol. Cell Biol.* 8:633–644. https://doi.org/10.1038/nrm2222

Lecuit, T., and A.S. Yap. 2015. E-cadherin junctions as active mechanical integrators in tissue dynamics. *Nat. Cell Biol.* 17:533–539. https://doi.org/10.1038/ncb3136

Letunic, I., T. Doerks, and P. Bork. 2015. SMART: recent updates, new developments and status in 2015. *Nucleic Acids Res.* 43:D257–D260. https://doi.org/10.1093/nar/gku949

Loie, E., L.E. Charrier, K. Sollier, J.Y. Masson, and P. Laprise. 2015. CRB3A Controls the Morphology and Cohesion of Cancer Cells through Ehm2/p114RhoGEF-Dependent Signaling. *Mol. Cell. Biol.* 35:3423–3435. https://doi.org/10.1128/MCB.00673-15

Luo, L., Y.J. Liao, L.Y. Jan, and Y.N. Jan. 1994. Distinct morphogenetic functions of similar small GTPases: Drosophila Drac1 is involved in axonal outgrowth and myoblast fusion. *Genes Dev.* 8:1787–1802. https://doi.org/10.1101/gad.8.15.1787

Mack, N.A., and M. Georgiou. 2014. The interdependence of the Rho GTPases and apicobasal cell polarity. *Small GTPases.* 5:e973968. https://doi.org/10.4161/21541248.2014.973768

Magie, C.R., M.R. Meyer, M.S. Gorsuch, and S.M. Parkhurst. 1999. Mutations in the Rho1 small GTPase disrupt morphogenesis and segmentation during early Drosophila development. *Development.* 126:5353–5364.

Manning, A.J., and S.L. Rogers. 2014. The Fog signaling pathway: insights into signaling in morphogenesis. *Dev. Biol.* 394:6–14. https://doi.org/10.1016/j.ydbio.2014.08.003

Matsuo, N., M. Terao, Y. Nabeshima, and M. Hoshino. 2003. Roles of STEF/Tiam1, guanine nucleotide exchange factors for Rac1, in regulation of growth cone morphology. *Mol. Cell. Neurosci.* 24:69–81. https://doi.org/10.1016/S1044-7431(03)00122-2

Matsuoka, T., and M. Yashiro. 2014. Rho/ROCK signaling in motility and metastasis of gastric cancer. *World J. Gastroenterol.* 20:13756–13766. https://doi.org/10.3748/wjg.v20.i38.13756

McCormack, J., N.J. Welsh, and V.M. Braga. 2013. Cycling around cell-cell adhesion with Rho GTPase regulators. *J. Cell Sci.* 126:379–391. https://doi.org/10.1242/jcs.097923

Munjal, A., J.M. Philippe, E. Munro, and T. Lecuit. 2015. A self-organized biomechanical network drives shape changes during tissue morphogenesis. *Nature.* 524:351–355. https://doi.org/10.1038/nature14603

Nakajima, H., and T. Tanoue. 2010. Epithelial cell shape is regulated by Lulu proteins via myosin-II. *J. Cell Sci.* 123:555–566. https://doi.org/10.1242/jcs.057752

Nakajima, H., and T. Tanoue. 2011. Lulu2 regulates the circumferential actomyosin tensile system in epithelial cells through p114RhoGEF. *J. Cell Biol.* 195:245–261. https://doi.org/10.1083/jcb.201104118

Nakajima, H., and T. Tanoue. 2012. The circumferential actomyosin belt in epithelial cells is regulated by the Lulu2-p114RhoGEF system. *Small GTPases.* 3:91–96. https://doi.org/10.4161/sgtp.19112

Ngok, S.P., W.H. Lin, and P.Z. Anastasiadis. 2014. Establishment of epithelial polarity--GEF who's minding the GAP? *J. Cell Sci.* 127:3205–3215. https://doi.org/10.1242/jcs.153197

Ni, J.Q., R. Zhou, B. Czech, L.P. Liu, L. Holderbaum, D. Yang-Zhou, H.S. Shim, R. Tao, D. Handler, P. Karpowicz, et al. 2011. A genome-scale shRNA resource for transgenic RNAi in Drosophila. *Nat. Methods.* 8:405–407. https://doi.org/10.1038/nmeth.1592

Padash Barmchi, M., S. Rogers, and U. Häcker. 2005. DRhoGEF2 regulates actin organization and contractility in the Drosophila blastoderm embryo. *J. Cell Biol.* 168:575–585. https://doi.org/10.1083/jcb.200407124

Pédelacq, J.D., S. Cabantous, T. Tran, T.C. Terwilliger, and G.S. Waldo. 2006. Engineering and characterization of a superfolder green fluorescent protein. *Nat. Biotechnol.* 24:79–88. https://doi.org/10.1038/nbt1172

Pellikka, M., G. Tanentzapf, M. Pinto, C. Smith, C.J. McGlade, D.F. Ready, and U. Tepass. 2002. Crumbs, the Drosophila homologue of human CRB1/RP12, is essential for photoreceptor morphogenesis. *Nature.* 416:143–149. https://doi.org/10.1038/nature721

Ratheesh, A., R. Priya, and A.S. Yap. 2013. Coordinating Rho and Rac: the regulation of Rho GTPase signaling and cadherin junctions. *Prog. Mol. Biol. Transl. Sci.* 116:49–68. https://doi.org/10.1016/B978-0-12-394311-8.00003-0

Rauzi, M., P.F. Lenne, and T. Lecuit. 2010. Planar polarized actomyosin contractile flows control epithelial junction remodelling. *Nature.* 468:1110–1114. https://doi.org/10.1038/nature09566

Ren, Y., R. Li, Y. Zheng, and H. Busch. 1998. Cloning and characterization of GEF-H1, a microtubule-associated guanine nucleotide exchange factor for Rac and Rho GTPases. *J. Biol. Chem.* 273:34954–34960. https://doi.org/10.1074/jbc.273.52.34954

Ridley, A.J. 2012. Historical overview of Rho GTPases. *Methods Mol. Biol.* 827:3–12.

Rørth, P. 1998. Gal4 in the Drosophila female germline. *Mech. Dev.* 78:113–118. https://doi.org/10.1016/S0925-4773(98)00157-9

Royou, A., W. Sullivan, and R.E. Karess. 1999. In vivo studies Drosophila nonmuscle myosin II tagged with Green Fluorescent Protein. *Mol. Biol. Cell.* 10:34.

Samarin, S.N., A.I. Ivanov, G. Flatau, C.A. Parkos, and A. Nusrat. 2007. Rho/Rho-associated kinase-II signaling mediates disassembly of epithelial apical junctions. *Mol. Biol. Cell.* 18:3429–3439. https://doi.org/10.1091/mbc.e07-04-0315

Schultz, J., F. Milpetz, P. Bork, and C.P. Ponting. 1998. SMART, a simple modular architecture research tool: identification of signaling domains. *Proc. Natl. Acad. Sci. USA.* 95:5857–5864. https://doi.org/10.1073/pnas.95.11.5857

Sen, A., Z. Nagy-Zsvér-Vadas, and M.P. Krahn. 2012. Drosophila PATJ supports adherens junction stability by modulating Myosin light chain activity. *J. Cell Biol.* 199:685–698. https://doi.org/10.1083/jcb.201206064

Shibolet, O., C. Giallourakis, I. Rosenberg, T. Mueller, R.J. Xavier, and D.K. Podolsky. 2007. AKAP13, a RhoA GTPase-specific guanine exchange factor, is a novel regulator of TLR2 signaling. *J. Biol. Chem.* 282:35308–35317. https://doi.org/10.1074/jbc.M704426200

Simões, S.M., J.T. Blankenship, O. Weitz, D.L. Farrell, M. Tamada, R. Fernandez-Gonzalez, and J.A. Zallen. 2010. Rho-kinase directs Bazooka/Par-3 planar polarity during Drosophila axis elongation. *Dev. Cell.* 19:377–388. https://doi.org/10.1016/j.devcel.2010.08.011

Simões, S.M., A. Mainieri, and J.A. Zallen. 2014. Rho GTPase and Shroom direct planar polarized actomyosin contractility during convergent extension. *J. Cell Biol.* 204:575–589. https://doi.org/10.1083/jcb.201307070

Strutt, D.I., U. Weber, and M. Mlodzik. 1997. The role of RhoA in tissue polarity and Frizzled signalling. *Nature.* 387:292–295. https://doi.org/10.1038/387292a0

Tanentzapf, G., and U. Tepass. 2003. Interactions between the crumbs, lethal giant larvae and bazooka pathways in epithelial polarization. *Nat. Cell Biol.* 5:46–52. https://doi.org/10.1038/ncb896

Tepass, U. 1996. Crumbs, a component of the apical membrane, is required for zonula adherens formation in primary epithelia of Drosophila. *Dev. Biol.* 177:217–225. https://doi.org/10.1006/dbio.1996.0157

Tepass, U. 2012. The apical polarity protein network in Drosophila epithelial cells: regulation of polarity, junctions, morphogenesis, cell growth, and survival. *Annu. Rev. Cell Dev. Biol.* 28:655–685. https://doi.org/10.1146/annurev-cellbio-092910-154033

Tepass, U., and E. Knust. 1993. Crumbs and stardust act in a genetic pathway that controls the organization of epithelia in Drosophila melanogaster. *Dev. Biol.* 159:311–326. https://doi.org/10.1006/dbio.1993.1243

Tepass, U., C. Theres, and E. Knust. 1990. crumbs encodes an EGF-like protein expressed on apical membranes of Drosophila epithelial cells and required for organization of epithelia. *Cell.* 61:787–799. https://doi.org/10.1016/0092-8674(90)90189-L

Tepass, U., E. Gruszynski-DeFeo, T.A. Haag, L. Omatyar, T. Török, and V. Hartenstein. 1996. shotgun encodes Drosophila E-cadherin and is preferentially required during cell rearrangement in the neurectoderm and other morphogenetically active epithelia. *Genes Dev.* 10:672–685. https://doi.org/10.1101/gad.10.6.672

Tepaß, U., and E. Knust. 1990. Phenotypic and developmental analysis of mutations at thecrumbs locus, a gene required for the development of epithelia inDrosophila melanogaster. *Rouxs Arch. Dev. Biol.* 199:189–206. https://doi.org/10.1007/BF01682078

Terry, S.J., C. Zihni, A. Elbediwy, E. Vitiello, I.V. Leefa Chong San, M.S. Balda, and K. Matter. 2011. Spatially restricted activation of RhoA signalling at epithelial junctions by p114RhoGEF drives junction formation and morphogenesis. *Nat. Cell Biol.* 13:159–166. https://doi.org/10.1038/ncb2156

Uemura, T., H. Oda, R. Kraut, S. Hayashi, Y. Kotaoka, and M. Takeichi. 1996. Zygotic Drosophila E-cadherin expression is required for processes of dynamic epithelial cell rearrangement in the Drosophila embryo. *Genes Dev.* 10:659–671. https://doi.org/10.1101/gad.10.6.659

Verboon, J.M., and S.M. Parkhurst. 2015. Rho family GTPase functions in Drosophila epithelial wound repair. *Small GTPases.* 6:28–35. https://doi.org/10.4161/21541248.2014.982415

Vichas, A., M.T. Laurie, and J.A. Zallen. 2015. The Ski2-family helicase Obelus regulates Crumbs alternative splicing and cell polarity. *J. Cell Biol.* 211:1011–1024. https://doi.org/10.1083/jcb.201504083

Wang, C., Y. Shang, J. Yu, and M. Zhang. 2012a. Substrate recognition mechanism of atypical protein kinase Cs revealed by the structure of PKCι in complex with a substrate peptide from Par-3. *Structure.* 20:791–801. https://doi.org/10.1016/j.str.2012.02.022

Wang, J.W., E.S. Beck, and B.D. McCabe. 2012b. A modular toolset for recombination transgenesis and neurogenetic analysis of Drosophila. *PLoS One.* 7:e42102. https://doi.org/10.1371/journal.pone.0042102

Wieschaus, E., and C. Nüsslein-Volhard. (1986). Looking at embryos. In: Roberts, DB, ed. *Drosophila: A practical approach.* IRL Press, Oxford, UK; 199–227.

Wodarz, A., U. Hinz, M. Engelbert, and E. Knust. 1995. Expression of crumbs confers apical character on plasma membrane domains of ectodermal epithelia of Drosophila. *Cell.* 82:67–76. https://doi.org/10.1016/0092-8674(95)90053-5

Zallen, J.A., and E. Wieschaus. 2004. Patterned gene expression directs bipolar planar polarity in Drosophila. *Dev. Cell.* 6:343–355. https://doi.org/10.1016/S1534-5807(04)00060-7